Kaposi's sarcoma-associated herpesvirus (KSHV) utilizes the NDP52/CALCOCO2 selective autophagy receptor to disassemble processing bodies

Short title: Selective targeting of processing bodies for autophagy by KSHV

inflammatory cytokine transcripts / Kaposi's sarcoma-associated herpesvirus / NDP52 / processing bodies / selective autophagy

Carolyn-Ann Robinson[1,2,3,4], Gillian K. Singh[1,4], Elizabeth L. Castle[1], Bre Q. Boudreau[1], Jennifer A. Corcoran[1,2,3,5]

[1]Department of Microbiology & Immunology, Dalhousie University, Halifax, NS, Canada
[2]Microbiology, Immunology & Infectious Diseases Department, University of Calgary, Calgary, AB, Canada.
[3]Charbonneau Cancer Research Institute, University of Calgary, Calgary, AB, Canada.
[4]Equal Contribution
[5]Corresponding Author

Abstract

Processing bodies (PBs) are cytoplasmic ribonucleoprotein granules that control inflammation by silencing or degrading labile messenger RNAs (mRNAs) that encode inflammatory molecules. PBs often disassemble in response to virus infection, which correlates with increased synthesis of inflammatory proteins. We previously showed that the Kaposi's sarcoma-associated herpesvirus (KSHV) KapB protein causes PB disassembly. Here, we reveal that PB disassembly mediated by KSHV or the viral protein KapB depends on the canonical autophagy genes *Atg5* and *Atg14* or the selective autophagy receptor *NDP52/CALCOCO2*. Moreover, KapB expression increased inflammatory transcripts levels and this effect was also dependent on canonical autophagy and NDP52. Stimulating autophagy with the mTOR inhibitor Torin-1 also increased cytokine mRNA and required ATG5 and NDP52 to mediate PB disassembly. These studies reveal a new role for NDP52 in regulating inflammatory responses by promoting PB turnover and the concomitant synthesis of inflammatory molecules.

16

17 **Introduction**

18 Macroautophagy, hereafter referred to as autophagy, is an evolutionarily conserved degradative
19 process that ensures the continuous recycling of material to maintain cellular homeostasis (1–3).
20 Autophagy begins with the formation of a phagophore that elongates and encloses a portion of
21 the cytoplasm to form a double-membrane specialized organelle, the autophagosome, which
22 fuses with lysosomes to form autolysosomes, where its contents are degraded (4). Under basal
23 conditions, autophagic activity ensures the clearance of damaged macromolecular complexes and
24 organelles, acting as an intracellular quality control system (2). Various changes to the cellular
25 microenvironment, including nutrient scarcity, hypoxia, and endoplasmic reticulum (ER) stress
26 can upregulate autophagy, reprioritizing resources and promoting cell survival during adverse
27 and stressful conditions (2).

28

29 Although previously considered a non-selective, bulk, degradative pathway of cytoplasmic
30 recycling, recent work shows differential cargo targeting by autophagy through a process known
31 as selective autophagy (5,6). Autophagy can selectively target specific cellular components,
32 including organelles (e.g mitochondria, peroxisomes, ER) and protein complexes (e.g.
33 ribosomes, focal adhesion complexes, protein aggregates) for degradation (5,7). In selective
34 autophagy, target cargo is selected either directly, by binding to lipidated microtubule associated
35 protein 1 light chain 3 (LC3) protein (LC3-II)/Atg8, or more commonly, via a receptor that
36 mediates cargo recognition. These molecular bridges are termed selective autophagy receptors
37 (SARs), and their role is to link the selected cargo to lipidated LC3-II molecules which are
38 anchored to the expanding phagophore (8). Some of the best characterized SARs include

39 p62/SQSTM1, valosin containing protein (VCP), optineurin (OPTN), neighbor of BRCA1 gene
40 1 (NBR1), nuclear dot protein 52 (NDP52/calcium binding and coiled-coil domain protein,
41 CALCOCO2) and its paralogue TAX1BP1/CALCOCO3 (5,9,10). Of these, OPTN, p62, NDP52,
42 and NBR1 are members of the sequestosome-like family and contain several conserved motifs
43 including a LC3-interacting region (LIR) and a ubiquitin-binding domain (UBD) to mediate
44 cargo selection via binding the ubiquitin chains present on the cargo surface (6,11–13). Roughly
45 half of the selective autophagy mechanisms described thus far rely on ubiquitination for cargo
46 selection, including the processes of mitophagy, xenophagy, and aggrephagy (5,11). In other
47 examples, such as ER-phagy, the involvement of ubiquitin modification in autophagosomal
48 targeting remains unclear (14).
49
50 While SARs play important homeostatic roles maintaining, and at times magnifying, the turnover
51 of organelles and aggregates via cargo selection, an emerging function of these receptors is to
52 localize the initiation of autophagy. SARs p62 and NDP52 both promote autophagosome
53 formation at the cargo site through a direct interaction with autophagic initiating complexes (15–
54 17). SARs also play important roles in fine-tuning innate immune responses by targeting key
55 signaling platforms for degradation (18–23). For example, NDP52 is required for the autophagic
56 degradation of interferon regulatory factor 3 (IRF3) and mitochondrial antiviral signaling protein
57 (MAVS), which supports the resolution phase of type I interferon signaling (24) (20,25). Both
58 pro- and antiviral roles have been attributed to SARs (26,27) and viruses can both enhance or
59 limit SAR function accordingly, promoting their replication (28).
60
61 Kaposi's sarcoma-associated herpesvirus (KSHV) is the infectious cause of two B-cell

62 malignancies and the endothelial cell cancer, Kaposi's sarcoma (KS), which is typified by
63 aberrant angiogenesis, tortuous leaky blood vessels, and inflammation (29–31). Infection with
64 KSHV has two forms, a latent and a lytic phase and it is the latent phase that predominates in KS
65 tumours (32–34). Like many viruses, KSHV manipulates the autophagic machinery. During
66 latency, the viral FLICE inhibitory protein (v-FLIP) binds Atg3 to suppress the LC3 lipidation
67 process during autophagosome biogenesis (35). KSHV also expresses a viral cyclin D homolog
68 (v-cyclin), that triggers DNA damage that leads to autophagy and cellular senescence (36),
69 facilitating the production and non-conventional secretion of pro-inflammatory cytokines such as
70 IL-1β, IL-6 and IL-8 (37). Together, KSHV manipulation of autophagic flux prevents
71 xenophagy, limits interferon responses, and enhances inflammatory cytokine production.
72 Precisely how KSHV fine tunes autophagy during latency to balance pro- and antiviral activities
73 and promote chronic viral infection is not clear.
74
75 Processing bodies (PBs) are ubiquitous, cytoplasmic, ribonucleoprotein (RNP) granules that
76 regulate expression of many cytokine RNA transcripts, making them important sites of
77 inflammatory control. PBs contain enzymes involved in mRNA turnover, including those that
78 mediate decapping (Dcp2; co-factors Dcp1a and Edc4/Hedls), 5'-3' exonucleolytic degradation
79 (5'-3' exonuclease Xrn1 and RNA helicase Rck/DDX6) and some components of the RNA-
80 induced silencing complex (28,38–43). mRNAs are routed to PBs for decay and/or repression by
81 RNA-binding proteins (RBPs) through recognition of common sequence elements (39). AU-rich
82 elements (AREs) are destablilizing RNA regulatory elements found in the 3' untranslated regions
83 of ~8% of cellular transcripts that are responsible for targeting RNAs to PBs (44–46). When
84 bound by destabilizing RBPs, ARE-containing RNAs are directed to PBs and suppressed (47–

85 49). Our group and others showed that microscopically visible PBs correlate with the constitutive
86 turnover or translational suppression of ARE-mRNAs; when PBs are dispersed, this suppression
87 is reversed (50–54). Because ARE-mRNAs code for potent regulatory molecules such as
88 inflammatory cytokines, PBs are important post-transcriptional sites of regulation that fine tune
89 the production of inflammatory cytokines whose transcripts contain AREs, including IL-6, IL-8,
90 IL-1β, and TNF (45,55–61).
91
92 PBs are dynamic structures that are continuously assembled and disassembled, yet relatively
93 little is known about how their activity is regulated. Stimuli that activate the p38/MK2 MAP
94 kinase pathway as well as many virus infections elicit PB disassembly and a concomitant
95 reduction in ARE-mRNA suppression to promote inflammatory molecule production
96 (50,51,54,62–64). We have previously shown that KSHV causes PB disassembly during latent
97 infection, and that the viral protein Kaposin B (KapB) induces PB disassembly while enhancing
98 the production of an ARE-containing reporter (51,62,65). These data support the notion that PB
99 disassembly is likely an important contributor to inflammation associated with KS (51,66).
100 Although we know that KapB binds and activates the kinase MK2, and that MK2 is an important
101 component of the mechanism of KapB-mediated PB disassembly and ARE-mRNA stabilization,
102 we do not precisely understand how PB loss is elicited by KapB (51,67). The observation that
103 MK2 can phosphorylate Beclin-1 to increase autophagic flux in response to nutrient scarcity (68)
104 suggested to us that KapB may drive autophagic flux through MK2. We now show that the
105 KSHV KapB protein enhances autophagic flux, revealing an additional layer of complexity in
106 viral regulation of autophagy during KSHV latency. We also show that KapB requires the
107 autophagy proteins Atg5 and Atg14 to induce PB disassembly and ARE-mRNA stabilization and

108 that KapB selects PB components for autophagic turnover using the selective autophagy
109 receptor, NDP52. Both Atg5 and NDP52 are also required for KSHV-induced PB disassembly
110 after infection. PB turnover is likewise elicited by the mTOR inhibitor and potent autophagy
111 inducer, Torin-1, and this process is also dependent on Atg5 and NDP52. By contrast, and
112 despite previous observations that it elicits PB disassembly and ARE-mRNA stabilization (51), a
113 constitutively active form of MK2 does not rely on selective autophagy machinery for PB loss.
114 Our data reveal that cells possess both autophagy-dependent and -independent mechanisms to
115 regulate PB turnover and inflammatory molecule production. These data also forge a new
116 connection between the selective autophagy receptor, NDP52, and cytoplasmic PBs, both of
117 which control innate immune responses and inflammation that is hijacked by the viral protein
118 KapB during KSHV latency.
119

120 **Results**

121 **KapB induces autophagic flux**

122 KapB expression activates the stress-responsive kinase MAPKAPK2 (MK2) (51,67). Since MK2
123 phosphorylates the essential autophagy inducer Beclin 1 in response to amino acid starvation
124 (68–70), we questioned whether KapB expression could promote autophagic flux. Essential for
125 autophagosome expansion is the lipidation of LC3 to form LC3-II, permitting its incorporation
126 into autophagosome membranes (71). To measure autophagic flux, we examined levels of LC3-
127 II and the SAR, p62, with and without treatment with the lysosomal inhibitor, Bafilomycin A1
128 (BafA1), as both LC3-II and p62 are also substrates for autophagy (72). To this end, human
129 umbilical vein endothelial cells (HUVECs) were transduced with lentiviral vectors that express
130 KapB or an empty vector control and treated for increasing times with BafA1; LC3-II and p62
131 accumulation in the presence or absence of BafA1 treatment was determined by immunoblotting.
132 When KapB-expressing cells were treated for 4 h with BafA1, the amount of LC3-II and p62
133 increased two- and four-fold, respectively, compared to untreated cells. Both proteins showed
134 higher accumulation after BafA1 treatment of KapB-expressing cells than equivalently treated
135 vector controls (Fig 1A), indicating that autophagic flux was specifically enhanced in KapB-
136 expressing cells. We also measured endogenous LC3 puncta using immunofluorescence as an
137 indicator of autophagic flux (73,74). Untreated KapB-expressing HUVECs displayed LC3
138 puncta area similar to that of control cells; however, LC3 puncta area increased after BafA1
139 treatment, further suggesting that KapB expression enhanced autophagic flux (Fig 1B). Taken
140 together, these data show that KapB expression induced autophagic flux in HUVECs.

141

142 **KapB-mediated PB disassembly requires Atg5 and Atg14**

143 Our group previously described that MK2 activation was an important component of KapB-
144 mediated PB loss (51); however, these experiments did not reveal the precise mechanism of PB
145 loss nor did they clarify if KapB was causing PB disassembly or blocking PB assembly. Since
146 PBs are dynamic RNP granules, we wanted to determine whether KapB-mediated PB loss was a
147 result of enhanced disassembly of PBs or prevention of their *de novo* assembly. To do so, we
148 utilized HeLa cells that express a Dox-inducible GFP-tagged version of the PB-resident protein,
149 Dcp1a (41). When fixed, GFP-positive puncta co-stain with endogenous PB proteins such as the
150 RNA helicase DDX6/Rck and the decapping co-factor Hedls/Edc4, indicating that they represent
151 PBs (Fig S1). KapB was transfected into these cells either before or after inducing GFP-Dcp1a
152 granule formation. When KapB was expressed prior to granule induction, Dcp1a puncta formed,
153 although appearance for GFP-positive puncta was delayed compared to vector control cells (Fig
154 S1A). In the presence of KapB, *de novo* PB assembly was not blocked; however, when KapB
155 was expressed after granule induction, GFP-positive puncta were lost (Fig S1B), indicating that
156 KapB expression induced PB disassembly. As further evidence that KapB does not prevent PB
157 formation, we treated KapB-expressing HUVECs with sodium arsenite, a known inducer of PB
158 assembly. We observed that sodium arsenite induced endogenous PB formation in KapB-
159 expressing HUVECs that was indistinguishable from equivalently treated control cells (Fig S1C).
160 Taken together, these results show that KapB expression caused PB disappearance by inducing
161 PB disassembly but did not block PB assembly. We speculated that KapB may be utilizing a
162 normal cellular pathway that mediates the turnover of RNPs or their components, such as
163 autophagy.
164

165 To determine if autophagy was required for KapB-mediated PB disassembly, we first inhibited
166 autophagic flux by independently silencing two autophagy genes, Atg5 and Atg14 (Fig S2A, B).
167 When either Atg5 or Atg14 were silenced in KapB-expressing HUVECs, PBs were restored,
168 whereas their silencing did not have an effect in control cells (Fig 1C and D). We then examined
169 the ability of KapB to mediate PB disassembly in Atg5 -/- MEFs, which are defective for
170 autophagy (75), as indicated by the lack of LC3-II (Fig S2C). KapB failed to disassemble PBs in
171 Atg5 -/- MEFs but did disassemble PBs in matched wild-type controls (Fig S2D). Moreover,
172 KapB expression resulted in a significant increase in Atg5 protein levels (Fig S2A), consistent
173 with our other data that show that KapB is promoting autophagy. Blocking autophagic
174 degradation with BafA1 also restored PBs in KapB-expressing cells (Fig 1E). These data suggest
175 that KapB is accelerating PB disassembly by enhancing autophagy.
176
177 Autophagy, although always occurring at a basal level, can be upregulated by many different cell
178 stimuli including starvation or inhibition of mTOR using Torin-1, hereafter referred to as Torin
179 (76). It was previously reported that rapamycin, an inhibitor of mTORC1, caused a loss of PBs in
180 mammary epithelial cells (77). We reasoned that if we inhibited both mTOR complexes
181 mTORC1 and mTORC2 using Torin (78) to induce autophagy, PBs would disassemble. We
182 observed that the number of Hedls/Edc4 puncta were significantly reduced after Torin treatment,
183 indicating that chemical induction of autophagy also resulted in the disappearance of PBs (Fig
184 2A). To ensure that Torin treatment was inducing disassembly of PBs and not preventing
185 assembly, HUVECs were treated with sodium arsenite to induce PB formation; like KapB, Torin
186 treatment did not prevent the assembly of PBs under these conditions (Fig 2B).
187

188 Given these similarities, we wondered if, like Torin, KapB induced autophagy was via inhibition
189 of mTOR complexes mTORC1 and mTORC2. To test this, we performed immunoblotting for
190 the phosphorylation of the ribosomal protein S6 (Serines 235/236), a known downstream target
191 of mTOR activation (79). Unlike Torin, KapB expression did not decrease phosphorylation of
192 S6 (Fig 2C). We also tested the ability of a constitutively active form of MK2 (two threonine
193 residues substituted with glutamic acid residues [T205E/T317E]; called MK2EE) (80–82). We
194 previously demonstrated that MK2EE caused PB disassembly (51) and others showed it
195 increased autophagic flux after starvation (68). Like KapB, MK2EE expression also did not
196 decrease phosphorylation of S6 (Fig 2C). These data indicate KapB does not inhibit mTOR
197 activity to induce autophagy. Since KapB can bind and activate MK2, we next wondered if
198 KapB expression would mediate phosphorylation of Beclin-1 at Serine 90, as shown for
199 MK2EE. Like MK2EE, KapB induced phosphorylation of Beclin-1 at Serine 90 (Fig 2D),
200 indicating that induction of autophagy via KapB expression is mediated by Beclin-1. Taken
201 together, these data show that although both KapB expression and Torin treatment caused PB
202 disassembly in an autophagy-dependent manner, the mechanism used to upregulate autophagic
203 flux differed in each case.
204

205 **Canonical autophagy is required for KapB-mediated increases in ARE-containing cytokine**
206 **transcripts**

207 PBs are nodes of mRNA regulation and microscopically visible PBs are associated with ARE-
208 mRNA decay or suppression (43,50,51,53,54,83,84). We treated HUVECs with conditioned
209 media from latent KSHV-infected cells to stimulate the transcription of inflammatory RNAs in a
210 biologically relevant manner and examined levels of some endogenous ARE-containing RNA

211 transcripts in KapB-expressing cells (Fig 3A). We observed significant increases of cytokine
212 mRNA for IL-6 and IL-1β in KapB-expressing cells compared to equivalently treated controls,
213 suggesting these increases resulted from reduced transcript decay in PBs (Fig 3A). In addition,
214 treatment with Torin promoted the enhanced steady-state levels of IL-1β and COX-2 (Fig 3B),
215 suggesting that inducing autophagy reduced the decay of some ARE-mRNA transcripts. To
216 support these findings and to simplify further studies, we utilized a luciferase reporter assay that
217 we developed, described in (65). Using this assay, we previously showed that KapB-mediated
218 PB loss correlated with enhanced luminescence of an ARE-containing firefly luciferase (Fluc)
219 reporter because its rapid turnover was reversed and FLuc translation was enhanced (51,65).
220 Briefly, HeLa cells were co-transfected with a FLuc construct containing the AU-rich element
221 from CSF2 in its 3'UTR and a Renilla luciferase (RLuc) construct with no ARE; transcription of
222 both reporter constructs was then stopped by the addition of doxycycline. In control (vector
223 transfected) cells, the FLuc-ARE mRNA decayed rapidly and FLuc luminescence relative to the
224 RLuc transfection control was low. Torin treatment caused a significant increase in FLuc/RLuc
225 relative luminescence compared to DMSO-treated control cells, supporting our RT-qPCR
226 findings (Fig 3C) and suggesting that enhanced autophagy reverses the constitutive
227 turnover/suppression of the ARE-mRNA reporter. Furthermore, KapB expression also caused a
228 significant increase in FLuc/RLuc relative luminescence compared to empty vector control cells
229 (Fig 3D) as previously shown in (51). When canonical autophagy was perturbed by either Atg5
230 or Atg14 silencing (Fig S3A, B) KapB-expressing cells had significantly decreased luminescence
231 compared to KapB-expressing controls (Fig 3D, E). Likewise, when KapB-expressing cells were
232 treated with BafA1, relative luminescence was significantly decreased compared to KapB-
233 expressing untreated control cells (Fig 3F). Together, these data showed that canonical

234 autophagy is required for KapB-mediated increases in cytokine mRNA levels and the enhanced
235 expression of an ARE-mRNA reporter.
236
237 **Dcp1a protein levels are decreased by KapB and Torin treatment**
238 Both KapB and Torin mediated PB disassembly but did not prevent *de novo* PB formation. We
239 reasoned that KapB and Torin could have this effect because they cause the autophagic
240 degradation of the entire PB granule. Alternately, since some PB proteins have important
241 scaffolding roles that hold granules together (EDC4/Hedls, Xrn1, DDX6/Rck, or Dcp1a (85)),
242 PB disassembly could be induced by KapB/Torin if one or more key PB proteins was missing
243 due to its accelerated degradation. To differentiate between these two scenarios, we performed
244 immunoblotting for PB proteins after Torin treatment and in the context of KapB expression (Fig
245 4). Immunoblotting revealed that steady-state levels of Dcp1a were reduced in Torin-treated (Fig
246 4A) and KapB-expressing cells (Fig 4B); however, steady-state levels of other PB-resident
247 proteins were not affected (Fig 4A, C). These data suggest that autophagy induction with Torin
248 or KapB expression promote the accelerated degradation of the PB-resident protein Dcp1a, but
249 not all PB proteins. Silencing the canonical autophagy gene, Atg5, resulted in a reversal of
250 KapB-mediated Dcp1a loss (Fig 4D), suggesting that autophagy is required for the loss of Dcp1a
251 observed after KapB expression.
252
253 **KapB-mediated PB disassembly and ARE-mRNA stabilization require the selective**
254 **autophagy receptor NDP52**
255 After establishing a link between KapB expression, autophagy, and PB disassembly, we
256 wondered what specific autophagy mechanisms were at work and if selective autophagy

257 receptors (SARs) were involved. One previous study observed the SAR, NDP52, partially co-
258 localized with some PB proteins (86). For this reason, we used RNA silencing to investigate
259 whether NDP52, p62, VCP, NBR1, or OPTN were required for KapB-mediated PB disassembly.
260 Despite trying several different shRNA sequences, our attempts to silence NBR1 were
261 unsuccessful, and shRNAs targeting VCP resulted in significant HUVEC toxicity (Fig S4A, B).
262 Therefore, the role of these molecules in KapB-mediated PB disassembly could not be
263 determined. Knockdown of NDP52, p62, and OPTN was validated in control and KapB-
264 expressing cells (Fig S4C-E). Silencing of p62 or OPTN did not restore PBs in KapB-expressing
265 cells whereas NDP52 knockdown significantly restored PBs (Fig 5A, Fig S4F). These data
266 pinpointed an important role for NDP52 and selective autophagy in KapB-mediated PB
267 disassembly. We then tested whether NDP52 silencing could prevent Torin-mediated PB
268 disassembly and found that PBs could not be disassembled in cells lacking NDP52 (Fig 5B,
269 S4G). We also examined whether these SARs were required for KapB-enhanced relative
270 luminescence in our ARE-mRNA reporter assay. We validated silencing of NDP52, p62, and
271 OPTN in HeLas (Fig S5A-C). Similarly, we found that p62 or OPTN knockdown had no effect
272 on KapB-mediated ARE-containing reporter luminescence, but NDP52 silencing decreased the
273 signal compared to non-targeting, KapB-expressing controls (Fig 5C), further supporting the role
274 of NDP52 in autophagy-mediated PB disassembly. We then performed an NDP52
275 complementation experiment. We first silenced endogenous NDP52 in control or KapB-
276 expressing HUVECs using shRNAs targeting the 3'UTR of NDP52 and verified its knockdown
277 (Fig S6A). Next, NDP52 expression was restored by overexpressing a fluorescently tagged
278 NDP52 construct. Complementation of NDP52-silenced HUVECs with wild-type NDP52
279 restored KapB-mediated PB disassembly compared to vector controls (Fig 5E, F; S6B, C).

280 Taken together, these data indicate that NDP52 is required for KapB- and Torin-mediated PB
281 disassembly and KapB-mediated ARE-mRNA stabilization.
282
283 **Atg5 and NDP52 are not required for MK2-mediated PB disassembly**
284 We previously demonstrated that MK2EE causes PB disassembly (51) and others have shown
285 that it can also increase autophagic flux (68). We confirmed that autophagy was upregulated in
286 MK2EE-expressing HUVECs by staining for endogenous LC3 puncta. We observed that BafA1
287 treatment resulted in a significant increase in LC3-puncta compared to vector controls, consistent
288 with enhanced autophagic flux (Fig 6A). Furthermore, MK2EE expression resulted in an
289 increased accumulation of LC3-II and p62 after Baf A1 treatment to block degradation (Fig 6B).
290 We then tested if MK2EE-induced PB disassembly was reliant on autophagic flux. MK2EE-
291 expressing HUVECs retained the ability to disassemble PBs after Atg5 silencing (Fig 6C, S7A).
292 MK2EE expression was previously shown to increase the FLuc/RLuc relative luminescence in
293 our reporter assay (51) and we reproduced these data herein (Fig 6D). However, Atg5 silencing
294 did not significantly decrease MK2EE-mediated relative luminescence (Fig 6D, S7B). These
295 data suggest that although MK2EE induces autophagy and PB disassembly, how MK2EE
296 induces PB disassembly does not require autophagy pathways involving Atg5.
297
298 Given that MK2 induces autophagy, but MK2EE-mediated PB disassembly did not require Atg5,
299 we speculated that MK2EE-mediated PB disassembly could be facilitated by NDP52. However,
300 p62, NDP52 and OPTN silencing did not inhibit PB disassembly in MK2EE-expressing cells
301 (Fig S7C-E; 6E; S7F). Likewise, silencing of p62, OPTN, or NDP52 did not decrease
302 FLuc/RLuc luminescence in MK2EE-expressing cells as it did in KapB-expressing cells (Fig 6F,

303 S7G-I). In fact, NDP52 knockdown increased ARE-mRNA stability (Fig 6F), although the
304 significance of this observation is unclear. These data confirm that MK2-mediated PB
305 disassembly and enhanced ARE-containing luciferase reporter expression do not require
306 canonical autophagy or selective autophagy machinery.
307
308 **Atg5 and NDP52 are required for KSHV-mediated PB disassembly**
309 Autophagy regulation during KSHV latency is complex, as multiple viral gene products
310 modulate autophagic flux in addition to KapB (35,36). We previously showed that KSHV
311 infection induced PB disassembly (51) and more recently we confirmed that KapB is not only
312 sufficient but also necessary for this effect in HUVECs (87). To determine if autophagic
313 machinery is also required for PB disassembly in the context of infection, HUVECs were
314 infected with the rKSHV.219 strain either treated or not with BafA1 for 30 minutes 96 hours
315 post infection, stained for PBs. Consistent with our data on KapB-induced PB disassembly,
316 blocking autophagic degradation with BafA1 also restored PBs in KSHV-infected cells (Fig 7A).
317 Moreover, RNA silencing of Atg5 and NDP52 also reversed KSHV-mediated PB disassembly
318 (Fig 7B). These data confirm an essential role for autophagy and the selective autophagy
319 receptor NDP52 in viral PB disassembly.
320
321 **Discussion**
322 Here we demonstrate that the KSHV protein, KapB, relies on selective autophagy to cause PB
323 disassembly and enhance ARE-mRNA stability. Furthermore, we identified NDP52 as the
324 selective autophagy receptor required for this process. To our knowledge, this is the first report
325 that NDP52 regulates the turnover of endogenous PBs and the first description of the

326 contribution of NDP52 to immune regulation by altering inflammatory cytokine RNA
327 turnover/suppression in PBs. We also show that PB disassembly induced by infection with
328 KSHV requires Atg5 and NDP52, suggesting an important role for elevated autophagic flux and
329 PB catabolism in regulating KSHV-associated inflammation. Our major findings are: i) KapB
330 increases autophagic flux, thereby contributing to the complex regulation of autophagic
331 processes during KSHV latent infection and tumourigenesis, ii) KapB-mediated PB disassembly
332 and enhanced translation of an ARE-containing reporter requires canonical autophagy machinery
333 and the selective autophagy receptor, NDP52, iii) Activation of autophagy by chemical inhibition
334 of mTORC1 using Torin causes PB disassembly using a mechanism that is dependent on
335 canonical autophagy and NDP52, suggesting that KapB manipulates an existing cellular pathway
336 that regulates PB catabolism, and iv) the mechanism of KapB- or Torin-mediated PB
337 disassembly differs from that induced by the constitutively active kinase, MK2 (MK2EE), which
338 is autophagy- and NDP52-independent. These results reveal that PB turnover is mediated by
339 autophagy-dependent and -independent mechanisms and shows that the viral KapB protein
340 hijacks a host pathway that uses NDP52 to enhance PB catabolism and promote inflammatory
341 molecule production.
342
343 MK2 activation promotes autophagy by phosphorylating Beclin 1 (68); therefore, we
344 hypothesized that KapB, an MK2-activating viral protein (67), would utilize autophagy to
345 promote PB clearance. Our data showed that although both KapB and MK2EE increased
346 autophagic flux via phosphorylating Beclin-1 at Serine 90 (Fig 1, 2, 6), only KapB-mediated PB
347 disassembly required the canonical autophagy proteins Atg5 and Atg14, and the selective
348 autophagy protein NDP52 (Fig 1, Fig 5). MK2EE does not use an autophagy-dependent

349 mechanism, as KapB does, for PB disassembly and our studies have not yet revealed a
350 mechanism for PB loss in these cells. These data imply that cells employ more than one pathway
351 to disassemble PBs, consistent with the dual mechanisms responsible for turnover of other RNP
352 granules like stress granules (88,89). Our data also suggest that KapB hijacks these two distinct
353 routes, an MK2-dependent pathway and an NDP52- and autophagy-dependent pathway to
354 disassemble PBs. This suggests PB loss is of central importance to KSHV latency. Our data are
355 supported by previous work showing that in yeast, PB recycling requires canonical autophagy
356 machinery, and in mammalian cells NDP52 colocalizes with a GFP-tagged version of Dcp1a
357 when overexpressed (86,88). We add significantly to these studies, by performing our work in
358 primary human endothelial cells and by staining for endogenous PBs using immunofluorescence
359 for the decapping co-factor Hedls/EDC4. We reveal that when KapB is expressed, endogenous
360 PBs are disassembled by an Atg5-, Atg14-, and NDP52-dependent autophagy process. We also
361 complemented NDP52-silenced cells with an shRNA-resistant NDP52 and observed the
362 restoration of KapB-mediated PB disassembly (Fig 5).
363
364 Immunoelectron microscopy showed that PBs range in size from 150 to 350 nm and possess an
365 external area of peripheral protrusions that contain the helicase Rck/DDX6 anchored to a dense
366 central core of decay enzymes, including Dcp1a and Xrn1 (38). Many PB-localized enzymes are
367 required for PB stability including Dcp1a; however, only three PB proteins are required for *de*
368 *novo* PB formation, DDX6, the translation suppressor, 4E-T, and LSM14a (85). Our data showed
369 that KapB expression decreased the steady-state levels of Dcp1a, while the steady-state levels of
370 other PB proteins were unaffected (Fig 4). Inducing autophagy with the mTORC1/2 inhibitor
371 Torin recapitulated this effect, decreasing steady-state levels of Dcp1a, but not other PB proteins

372 (Fig 4). These data support a model where the entire PB granule is not degraded by autophagy,
373 but PB disassembly is induced by the selective degradation of Dcp1a or another unidentified PB
374 protein. Consistent with this, we show that PBs can still form during KapB expression if we
375 overexpress Dcp1a-GFP or block translation using sodium arsenite (Fig S1). Dcp1a is also a
376 target for other viruses that mediate PB disassembly; for example, infection with poliovirus also
377 caused PB disassembly and the loss of Dcp1a over a time course of infection (90). We do not yet
378 understand how KapB expression or Torin treatment alters Dcp1a to promote its degradation and
379 the resultant PB disassembly, but we speculate that modulation of known post-translational
380 modifications of Dcp1a, such as phosphorylation or ubiquitination, may be involved (91–97).
381
382 In viral cancers like KS, autophagic flux promotes a pro-tumourigenic and pro-inflammatory
383 environment (98–101). The data shown herein brings new understanding to this complex
384 relationship during KSHV infection. We show that KapB induces autophagic flux and NDP52
385 selective autophagy of PBs, thereby supporting the pro-inflammatory environment associated
386 with latent KSHV infection and KS. We confirm that autophagy machinery and NDP52 are
387 required for PB disassembly during KSHV infection. The manipulation of NDP52 function and
388 autophagic flux by KSHV and KapB is yet another example of the ingenuity with which viruses
389 usurp cellular processes; revealing a regulatory network that links NDP52 to inflammatory
390 molecule production via PB catabolism.
391

392 **Materials and Methods**

393 **Cell culture**

394 All cells were grown at 37 °C with 5% CO_2 and 20% O_2. HEK293T cells (ATCC), HeLa Tet-Off
395 cells (Clontech), Atg5 +/+ and -/- MEFs (102), HeLa Flp-In TREx GFP-Dcp1a cells (a generous
396 gift from Anne-Claude Gingras), and iSLK.219 cells (a generous gift from Don Ganem) (103)
397 were cultured in DMEM (Thermo Fisher) supplemented with 100 U/mL penicillin, 100 µg/mL
398 streptomycin, 2 mM L-glutamine (Thermo Fisher) and 10% FBS (Thermo Fisher). iSLK.219
399 cells were additionally cultured in the presence of puromycin (10 µg/mL). HUVECs (Lonza)
400 were cultured in endothelial cell growth medium (EGM-2) (Lonza). HUVECs were seeded onto
401 gelatin (1% w/v in PBS)-coated tissue culture plates or glass coverslips. All drug treatments were
402 performed for the times indicated in each experiment at the concentrations listed in Table 1.

403 **Cloning**

404 All plasmids used in this study can be found in Table 2. All shRNAs were generated by cloning
405 shRNA hairpin sequences found in Table 3 into pLKO.1-TRC Puro (pLKO.1-TRC cloning
406 vector was a gift from David Root (Addgene plasmid # 10878; http://n2t.net/addgene:10878;
407 RRID:Addgene_10878) or pLKO.1-blast (pLKO.1-blast was a gift from Keith Mostov (Addgene
408 plasmid #26655; http://n2t.net/addgene:26655; RRID:Addgene_26655).

409 **Lentivirus Production and Transduction**

410 All lentiviruses were generated using a second-generation system. Briefly, HEK293T cells were
411 transfected with pSPAX2, MD2G, and the plasmid containing a gene of interest or hairpin using
412 polyethylimine (PEI, Polysciences). psPAX2 was a gift from Didier Trono (Addgene plasmid
413 #12260; http://n2t.net/addgene:12260; RRID:Addgene_12260) and pMD2.G was a gift from
414 Didier Trono (Addgene plasmid #12259; http://n2t.net/addgene:12259; RRID:Addgene_12259).

415

416 Viral supernatants were harvested 48 h post-transfection, clarified using a 0.45 µ
417 polyethersulfone filter (VWR), and frozen at -80°C until use. For transduction, lentiviruses were
418 thawed at 37°C and added to target cells in complete media containing 5 µg/mL polybrene
419 (Sigma) for 24 h. The media was changed to selection media containing 1 µg/mL puromycin or 5
420 µg/mL blasticidin (Thermo) and cells were selected for 48 h before proceeding with
421 experiments.

422 **Viral conditioned media treatments**

423 iSLK.219 cells (latently infected with rKSHV.219 virus) were sub-cultured into a 10 cm cell
424 culture dish and grown without puromycin for 72 h. At 72 h, conditioned media was reserved
425 and cleared of cellular debris by centrifugation at 500 G for 5 min. Supernatant was collected
426 and filtered through a 0.22 µM polyethersulfone (PES) membrane filter (VWR) and stored in
427 aliquots at -80. Prior to the experiment, conditioned media was thawed at 37°C and combined
428 1:1 with fresh HUVEC EGM-2 media and used to treat vector or KapB-expressing HUVECs for
429 0 or 6 h prior to total RNA harvest.

430 **Production of rKSHV.219 virus**

431 iSLK.219 cells were sub-cultured into a 10 cm cell culture dish without puromycin and
432 reactivated from latency with 1 µg/mL doxycycline (Sigma-Aldrich) and 1 mM sodium butyrate
433 (Sigma-Aldrich). After 72 h, supernatants were collected, centrifuged to remove cellular debris,
434 aliquoted, and stored at -80°C until use.

435 ***De novo* infection of HUVECs**

436 Sub-confluent (50-70%) 12-well plates of HUVECs were incubated with rKSHV.219 viral
437 inoculum diluted in antibiotic and serum free DMEM containing 5 µg/mL polybrene. Plates were

438 centrifuged at 800 x *g* for 2 hours at room temperature (105), the inoculum was removed and
439 replaced with either EGM-2.

440 **Immunofluorescence**

441 Cells were seeded onto coverslips for immunofluorescence experiments and fixed for 10 mins at
442 37 °C in 4% (v/v) paraformaldehyde (Electron Microscopy Sciences). Samples were
443 permeabilized with 0.1% (v/v) Triton X-100 (Sigma-Aldrich) for 10 min at room temperature
444 and blocked in 1% human AB serum (Sigma-Aldrich) for 1 h at room temperature. For
445 autophagosome immunofluorescence cells were fixed for 10 min in ice cold methanol at -20 °C
446 and blocked in 1% human AB serum for 1 h at room temperature. Primary and secondary
447 antibodies were diluted in 1% human AB serum and used at the concentrations in Table 4.
448 Samples were mounted with Prolong Gold AntiFade mounting media (Thermo). For CellProfiler
449 quantification of puncta, samples were incubated with WGA AlexaFluor-647 at a 1:400 dilution
450 for 10 min prior to permeabilization. Image analysis was performed using CellProfiler
451 (cellprofiler.org), an open source platform for image analysis (Carpenter et al., 2006);
452 quantification of puncta was performed as previously described, with the exception that cells
453 were defined by propagating out a set number of pixels from each nucleus (106).

454 **Immunoblotting**

455 Cells were lysed in 2x Laemmli buffer and stored at -20°C until use. The DC Protein Assay
456 (Bio-Rad) was used to quantify protein concentration as per the manufacturer's instructions. 10-
457 15 µg of protein lysate was resolved by SDS-PAGE on TGX Stain-Free acrylamide gels
458 (BioRad). Total protein images were acquired from the PVDF membranes after transfer on the
459 ChemiDoc Touch Imaging system (BioRad). Membranes were blocked in 5% bovine serum
460 albumin (BSA) or skim milk in Tris-buffered saline-Tween20 (TBS-T). Primary and secondary

461 antibodies were diluted in 2.5% BSA or skim milk, dilutions can be found in Table 4.
462 Membranes were visualized using Clarity Western ECL substrate and the ChemiDoc Touch
463 Imaging system (BioRad).

464 **Luciferase Assays**

465 Luciferase assays were performed as previously described (65). HeLa Tet-Off cells were
466 transduced with recombinant lentivirus expressing different shRNAs and selected. Cells were
467 transfected according to Corcoran *et al.* (2011) with pTRE2 Firefly Luciferase ARE, pTRE2
468 Renilla Luciferase, and the expression plasmid of interest using Fugene HD (Promega).
469 Luciferase and renilla activity were quantified using the Dual Luciferase Assay Kit (Promega)
470 and read on a GloMax multi-detection system (Promega).

471 **Quantitative PCR**

472 RNA was collected using a RNeasy Plus Mini Kit (Qiagen) according to the manufacturer's
473 instructions and stored at -80°C until further use. RNA concentration was determined and was
474 reverse transcribed using Maxima H Minus First Strand cDNA Synthesis Kit (Thermo Fisher)
475 using a combination of random and oligo (dT) primers according to the manufacturer's
476 instructions. cDNA was diluted 1:5 for all qPCR experiments and GoTaq qPCR Master Mix
477 (Promega) was used to amplify cDNA. The ΔΔquantitation cycle (Cq) method was used to
478 determine the fold change in expression of target transcripts. qPCR primer sequences can be
479 found in Table 5.

480 **Statistics**

481 Data shown are the mean ± standard error of the mean (SEM). Statistical significance was
482 determined using a one-way ANOVA, a 2-way ANOVA or Student's t-test when appropriate
483 with the applicable post-test (indicated in the corresponding figure legends). For ANOVAs,

484 matched data from each replicate was paired for analysis. All statistics were performed using
485 GraphPad Prism v.9.0.
486

487 **Acknowledgements**

488 The authors would like to dedicate this manuscript to Dr. Beth Levine, who was a leader in the
489 field of autophagy and viruses and who inspired this work. We sincerely thank the members of
490 the Corcoran lab for helpful discussions about this work. We would like to thank Dr. Craig
491 McCormick (Dalhousie University), Dr. Eric Pringle (Dalhousie University), and Dr. Andrew
492 Leidal (UCSF) for valuable feedback on this manuscript and the McCormick lab for plasmids,
493 expertise, and advice. We would like to thank Mr. Stephen Whitefield and Ms. Mary Ann
494 Trevors in the Dalhousie *CORES* (Cellular and Molecular Digital Imaging and Electron
495 Microscopy core facilities) and Dr. Anne Vaahtokari of the Charbonneau Microscopy Facility,
496 UCalgary for microscopy support. We would like to thank Dr. Andreas Till (University of
497 Bonn), Dr. Anne-Claude Gingras (Lunenfeld-Tanenbaum Research Institute) and Dr. Don
498 Ganem (Novartis) for sharing valuable reagents. Model figure created with BioRender. GKS was
499 supported by a CIHR CGS-M scholarship and Scotia Scholars NSHRF graduate training award.
500 ELC was supported by a Killam predoctoral scholarship, an NSERC CGS-M scholarship, and a
501 Nova Scotia Graduate scholarship. Operating funds to support this work derive from a CIHR
502 Project Grant PJT-153210 to JAC.
503

504 **Author Contributions**

505 Carolyn-Ann Robinson: Conceptualization, Experimentation, Analysis, Paper Writing
506 Gillian K. Singh: Conceptualization, Experimentation, Analysis, Paper Writing

Elizabeth L. Castle: Analysis

Bre Q. Boudreau: Experimentation

Jennifer A. Corcoran: Conceptualization, Experimentation, Supervision, Funding Acquisition, Project Administration, Paper Writing

Conflict of Interest

The authors have no competing interests to declare.

516 **References**
517
518 1. Dikic I, Elazar Z. Mechanism and medical implications of mammalian autophagy. Nat
519 Rev Mol Cell Biol. 2018;19:349–64.
520 2. Levine B, Kroemer G. Biological Functions of Autophagy Genes: A Disease Perspective.
521 Cell. 2019;176: 11-42.
522 3. Morishita H, Mizushima N. Diverse cellular roles of autophagy. Ann Rev Cell Dev Biol.
523 2019;35: 453–75.
524 4. Lawrence RE, Zoncu R. The lysosome as a cellular centre for signalling, metabolism and
525 quality control. Nat Cell Biol. 2019;21: 133-142.
526 5. Beese CJ, Brynjólfsdóttir SH, Frankel LB. Selective Autophagy of the Protein
527 Homeostasis Machinery: Ribophagy, Proteaphagy and ER-Phagy. Front Cell Dev Biol.
528 2020;7: 373.
529 6. Johansen T, Lamark T. Selective Autophagy: ATG8 Family Proteins, LIR Motifs and
530 Cargo Receptors. J Mol Biol. 2020;432: 80-103.
531 7. Kirkin V, Rogov V V. A Diversity of Selective Autophagy Receptors Determines the
532 Specificity of the Autophagy Pathway. Mol Cell. 2019;76: 268-285.
533 8. Rogov V, Dötsch V, Johansen T, Kirkin V. Interactions between Autophagy Receptors
534 and Ubiquitin-like Proteins Form the Molecular Basis for Selective Autophagy. Mol Cell.
535 2014;53:167–78.
536 9. Tumbarello DA, Manna PT, Allen M, Bycroft M, Arden SD, Kendrick-Jones J, et al. The
537 Autophagy Receptor TAX1BP1 and the Molecular Motor Myosin VI Are Required for
538 Clearance of Salmonella Typhimurium by Autophagy. PLoS Pathog. 2015;11: e1005174.
539 10. Sarraf SA, Shah H V., Kanfer G, Pickrell AM, Holtzclaw LA, Ward ME, et al. Loss of

540 TAX1BP1-Directed Autophagy Results in Protein Aggregate Accumulation in the Brain.
541 Mol Cell. 2020;80: 779-795.
542 11. Khaminets A, Behl C, Dikic I. Ubiquitin-Dependent And Independent Signals In Selective
543 Autophagy. Trends Cell Biol. 2016;26:6–16.
544 12. Rogov V V, Stolz A, Ravichandran AC, Rios-Szwed DO, Suzuki H, Kniss A, et al.
545 Structural and functional analysis of the GABARAP interaction motif (GIM). EMBO Rep.
546 2017;18: 1382-1396.
547 13. Marshall RS, Hua Z, Mali S, McLoughlin F, Vierstra RD. ATG8-Binding UIM Proteins
548 Define a New Class of Autophagy Adaptors and Receptors. Cell. 2019;177: 776-781.
549 14. Wilkinson S. ER-phagy: shaping up and destressing the endoplasmic reticulum. FEBS J.
550 2019;286: 2645-2663.
551 15. Ravenhill BJ, Boyle KB, von Muhlinen N, Ellison CJ, Masson GR, Otten EG, et al. The
552 Cargo Receptor NDP52 Initiates Selective Autophagy by Recruiting the ULK Complex to
553 Cytosol-Invading Bacteria. Mol Cell. 2019;74:320-329.
554 16. Turco E, Witt M, Abert C, Bock-Bierbaum T, Su MY, Trapannone R, et al. How
555 RB1CC1/FIP200 claws its way to autophagic engulfment of SQSTM1/p62-ubiquitin
556 condensates. Autophagy. 2019;15:1475-1477.
557 17. Vargas JNS, Wang C, Bunker E, Hao L, Maric D, Schiavo G, et al. Spatiotemporal
558 Control of ULK1 Activation by NDP52 and TBK1 during Selective Autophagy. Mol Cell.
559 2019;74: 347-362.
560 18. Chen M, Meng Q, Qin Y, Liang P, Tan P, He L, et al. TRIM14 Inhibits cGAS
561 Degradation Mediated by Selective Autophagy Receptor p62 to Promote Innate Immune
562 Responses. Mol Cell. 2016;64: 105–119.

563 19. Du Y, Duan T, Feng Y, Liu Q, Lin M, Cui J, et al. LRRC25 inhibits type I IFN signaling
564 by targeting ISG15-associated RIG-I for autophagic degradation. EMBO J. 2018;37: 351–
565 366.
566 20. Jin S, Tian S, Luo M, Xie W, Liu T, Duan T, et al. Tetherin Suppresses Type I Interferon
567 Signaling by Targeting MAVS for NDP52-Mediated Selective Autophagic Degradation in
568 Human Cells. Mol Cell. 2017;6: 308-322.
569 21. Prabakaran T, Bodda C, Krapp C, Zhang B, Christensen MH, Sun C, et al. Attenuation of
570 c GAS - STING signaling is mediated by a p62/ SQSTM 1-dependent autophagy pathway
571 activated by TBK1 . EMBO J. 2018;37: e97858.
572 22. Yang Q, Liu TT, Lin H, Zhang M, Wei J, Luo WW, et al. TRIM32-TAX1BP1-dependent
573 selective autophagic degradation of TRIF negatively regulates TLR3/4-mediated innate
574 immune responses. PLoS Pathog. 2017;13: e1006600.
575 23. He X, Zhu Y, Zhang Y, Geng Y, Gong J, Geng J, et al. RNF 34 functions in immunity
576 and selective mitophagy by targeting MAVS for autophagic degradation . EMBO J.
577 2019;38: e100978.
578 24. Wu Y, Jin S, Liu Q, Zhang Y, Ma L, Zhao Z, et al. Selective autophagy controls the
579 stability of transcription factor IRF3 to balance type I interferon production and immune
580 suppression. Autophagy. 2020;17: 1379-1392.
581 25. Seth RB, Sun L, Ea CK, Chen ZJ. Identification and characterization of MAVS, a
582 mitochondrial antiviral signaling protein that activates NF-κB and IRF3. Cell. 2005;122:
583 669–682.
584 26. Sumpter R, Levine B. Selective autophagy and viruses. Autophagy. 201; 7: 260–5.
585 27. Ahmad L, Mostowy S, Sancho-Shimizu V. Autophagy-virus interplay: From cell biology

586 to human disease. Front Cell Dev Biol. 2018;6: 155.
587 28. Mohamud Y, Qu J, Xue YC, Liu H, Deng H, Luo H. CALCOCO2/NDP52 and
588 SQSTM1/p62 differentially regulate coxsackievirus B3 propagation. Cell Death Differ.
589 2019;26: 1062–1076.
590 29. Cesarman E, Chang Y, Moore PS, Said JW, Knowles DM. Kaposi's sarcoma-associated
591 herpesvirus-like DNA sequences in AIDS-related body-cavity-based lymphomas. N Engl
592 J Med. 1995 May;332: 1186–1191.
593 30. Chang Y, Cesarman E, Pessin MS, Lee F, Culpepper J, Knowles DM, et al. Identification
594 of herpesvirus-like DNA sequences in AIDS-associated Kaposi's sarcoma. Science.
595 1994;266: 1865–1869.
596 31. Soulier J, Grollet L, Oksenhendler E, Cacoub P, Cazals-Hatem D, Babinet P, et al.
597 Kaposi's sarcoma-associated herpesvirus-like DNA sequences in multicentric Castleman's
598 disease. Blood. 1995; 86: 1276–1280.
599 32. Decker LL, Shankar P, Khan G, Freeman RB, Dezube BJ, Lieberman J, et al. The Kaposi
600 sarcoma-associated herpesvirus (KSHV) is present as an intact latent genome in KS tissue
601 but replicates in the peripheral blood mononuclear cells of KS patients. J Exp Med.
602 1996;184: 283–288.
603 33. Staskus KA, Zhong W, Gebhard K, Herndier B, Wang H, Renne R, et al. Kaposi's
604 sarcoma-associated herpesvirus gene expression in endothelial (spindle) tumor cells. J
605 Virol. 1997;71: 715–719.
606 34. Broussard G, Damania B. Regulation of KSHV Latency and Lytic Reactivation. Viruses.
607 2020;12: 1034.
608 35. Lee J-S, Li Q, Lee J-Y, Lee S-H, Jeong JH, Lee H-R, et al. FLIP-mediated autophagy

609 regulation in cell death control. Nat Cell Biol. 2009;11: 1355–1362.
610 36. Leidal AM, Cyr DP, Hill RJ, Lee PWK, McCormick C. Subversion of autophagy by
611 Kaposi's sarcoma-associated herpesvirus impairs oncogene-induced senescence. Cell
612 Host Microbe. 2012;11:167–180.
613 37. Young ARJ, Narita M, Ferreira M, Kirschner K, Sadaie M, Darot JFJ, et al. Autophagy
614 mediates the mitotic senescence transition. Genes Dev. 2009;23: 798–803.
615 38. Cougot N, Cavalier A, Thomas D, Gillet R. The Dual Organization of P-bodies Revealed
616 by Immunoelectron Microscopy and Electron Tomography. J Mol Biol. 2012;420:17–28.
617 39. Hubstenberger A, Courel M, Bénard M, Souquere S, Ernoult-Lange M, Chouaib R, et al.
618 P-Body Purification Reveals the Condensation of Repressed mRNA Regulons. Mol Cell.
619 2017;68: 144-157.
620 40. Corbet GA, Parker R. RNP granule formation: Lessons from P-bodies and stress granules.
621 Cold Spring Harb Symp Quant Biol. 2019;84: 203–215.
622 41. Youn JY, Dunham WH, Hong SJ, Knight JDR, Bashkurov M, Chen GI, et al. High-
623 Density Proximity Mapping Reveals the Subcellular Organization of mRNA-Associated
624 Granules and Bodies. Mol Cell. 2018;69: 517-532.
625 42. Riggs CL, Kedersha N, Ivanov P, Anderson P. Mammalian stress granules and P bodies at
626 a glance. J Cell Sci. 2020;133: jcs242487.
627 43. Luo Y, Na Z, Slavoff SA. P-Bodies: Composition, Properties, and Functions.
628 Biochemistry. 2018;57: 2424.
629 44. Barreau C, Paillard L, Osborne HB. AU-rich elements and associated factors: Are there
630 unifying principles? Nucleic Acids Res. 2005;33: 7138–7150.
631 45. Bakheet T, Hitti E, Khabar KSA. ARED-Plus: An updated and expanded database of AU-

632 rich element-containing mRNAs and pre-mRNAs. Nucleic Acids Res. 2018;46: D218–
633 220.
634 46. García-Mauriño SM, Rivero-Rodríguez F, Velázquez-Cruz A, Hernández-Vellisca M,
635 Díaz-Quintana A, De la Rosa MA, et al. RNA binding protein regulation and cross-talk in
636 the control of AU-rich mRNA Fate. Front Mol Biosci. 2017;4: 71.
637 47. Maitra S, Chou CF, Luber CA, Lee KY, Mann M, Chen CY. The AU-rich element mRNA
638 decay-promoting activity of BRF1 is regulated by mitogen-activated protein kinase-
639 activated protein kinase 2. RNA. 2008;14: 950–959.
640 48. Lai WS, Carballo E, Strum JR, Kennington EA, Phillips RS, Blackshear PJ. Evidence that
641 Tristetraprolin Binds to AU-Rich Elements and Promotes the Deadenylation and
642 Destabilization of Tumor Necrosis Factor Alpha mRNA. Mol Cell Biol. 1999;19: 4311–
643 4323.
644 49. Lai WS, Blackshear PJ. Interactions of CCCH zinc finger proteins with mRNA.
645 Tristetraprolin-mediated AU-rich element-dependent mRNA degradation can occur in the
646 absence of a poly(A) tail. J Biol Chem. 2001;276: 23144–23154.
647 50. Corcoran JA, Khaperskyy DA, Johnston BP, King CA, Cyr DP, Olsthoorn A V., et al.
648 Kaposi's Sarcoma-Associated Herpesvirus G-Protein-Coupled Receptor Prevents AU-
649 Rich-Element-Mediated mRNA Decay. J Virol. 2012;86: 8859–8871.
650 51. Corcoran JA, Johnston BP, McCormick C. Viral activation of MK2-hsp27-p115RhoGEF-
651 RhoA signaling axis causes cytoskeletal rearrangements, p-body disruption and ARE-
652 mRNA stabilization. PLoS Pathog. 2015;11: e1004597.
653 52. Franks TM, Lykke-Andersen J. TTP and BRF proteins nucleate processing body
654 formation to silence mRNAs with AU-rich elements. Genes Dev. 2007;21: 719–735.

655 53. Blanco FF, Sanduja S, Deane NG, Blackshear PJ, Dixon D a. Transforming growth factor
656 β regulates P-body formation through induction of the mRNA decay factor tristetraprolin.
657 Mol Cell Biol. 2014;34: 180–195.
658 54. Vindry C, Marnef A, Broomhead H, Twyffels L, Ozgur S, Stoecklin G, et al. Dual RNA
659 Processing Roles of Pat1b via Cytoplasmic Lsm1-7 and Nuclear Lsm2-8 Complexes. Cell
660 Rep. 2017;20:1187–1200.
661 55. Ensoli B, Nakamura S, Salahuddin SZ, Biberfeld P, Larsson L, Beaver B, et al. AIDS-
662 Kaposi's Sarcoma-Derived Cells Express Cytokines with Autocrine and Paracrine Growth
663 Effects. Science. 2010;243: 223–226.
664 56. Ensoli B, Stürzl M. Kaposi's sarcoma: a result of the interplay among inflammatory
665 cytokines, angiogenic factors and viral agents. Cytokine Growth Factor Rev. 1998;9: 63–
666 83.
667 57. Lane BR, Liu J, Bock PJ, Schols D, Coffey MJ, Strieter RM, et al. Interleukin-8 and
668 growth-regulated oncogene alpha mediate angiogenesis in Kaposi's sarcoma. J Virol.
669 2002;76: 11570–11583.
670 58. Miles SA, Rezai AR, Salazar-González JF, Vander Meyden M, Stevens RH, Logan DM,
671 et al. AIDS Kaposi sarcoma-derived cells produce and respond to interleukin 6. Proc Natl
672 Acad Sci U S A. 1990;87: 4068–4072.
673 59. Riva G, Barozzi P, Torelli G, Luppi M. Immunological and Inflammatory Features of
674 Kaposi's Sarcom and Other Kaposi's Sarcoma-Associated Herpesvirus/Human
675 Herpesvirus 8-Associated Neoplasias. AIDS Rev. 2010;9: 25–39.
676 60. Sadagopan S, Sharma-Walia N, Veettil MV, Raghu H, Sivakumar R, Bottero V, et al.
677 Kaposi's Sarcoma-Associated Herpesvirus Induces Sustained NF-κB Activation during

678 De Novo Infection of Primary Human Dermal Microvascular Endothelial Cells That Is
679 Essential for Viral Gene Expression. J Virol. 2007;81: 3949–3968.
680 61. Salahuddin S, Nakamura S, Biberfeld P, Kaplan M, Markham P, Larsson L, et al.
681 Angiogenic properties of Kaposi's sarcoma-derived cells after long-term culture in vitro.
682 Science. 1988;242: 430–433.
683 62. Corcoran JA, McCormick C. Viral activation of stress-regulated Rho-GTPase signaling
684 pathway disrupts sites of mRNA degradation to influence cellular gene expression. Small
685 GTPases. 2015;6: 178–185.
686 63. Standart N, Weil D. P-Bodies: Cytosolic Droplets for Coordinated mRNA Storage. Trends
687 Genet. 2018;34: 612–626.
688 64. Docena G, Rovedatti L, Kruidenier L, Fanning Á, Leakey NAB, Knowles CH, et al.
689 Down-regulation of p38 mitogen-activated protein kinase activation and proinflammatory
690 cytokine production by mitogen-activated protein kinase inhibitors in inflammatory bowel
691 disease. Clin Exp Immunol. 2010;162: 108–115.
692 65. Corcoran JA, Khaperskyy DA, McCormick C. Assays for monitoring viral manipulation
693 of host ARE-mRNA turnover. Methods. 2011;55: 172–181.
694 66. Wen KW, Damania B. Kaposi sarcoma-associated herpesvirus (KSHV): molecular
695 biology and oncogenesis. Cancer Lett. 2010;289: 140–150.
696 67. McCormick C, Ganem D. The Kaposin B Protein of KSHV Activates the p38/MK2
697 Pathway and Stabilizes Cytokine mRNAs. Science. 2005;307: 739–741.
698 68. Wei Y, An Z, Zou Z, Sumpter R, Su M, Zang X, et al. The stress-responsive kinases
699 MAPKAPK2/MAPKAPK3 activate starvation-induced autophagy through Beclin 1
700 phosphorylation. Elife. 2015;4: e05289.

701 69. Shen L, Qi Z, Zhu Y, Song X, Xuan C, Ben P, et al. Phosphorylated heat shock protein 27
702 promotes lipid clearance in hepatic cells through interacting with STAT3 and activating
703 autophagy. Cell Signal. 2016;28: 1086–1098.
704 70. Gurkar AU, Chu K, Raj L, Bouley R, Lee S-H, Kim Y-B, et al. Identification of ROCK1
705 kinase as a critical regulator of Beclin1-mediated autophagy during metabolic stress. Nat
706 Commun. 2013;4: 2189.
707 71. Klionsky DJ, Abdel-Aziz AK, Abdelfatah S, Abdellatif M, Abdoli A, Abel S, et al.
708 Guidelines for the use and interpretation of assays for monitoring autophagy (4th
709 edition)[1]. Autophagy. 2021;17: 1-382.
710 72. Mizushima N, Murphy LO. Autophagy Assays for Biological Discovery and Therapeutic
711 Development. Trends Biochem Sci. 2020;45: 1080-1093.
712 73. Mizushima N, Yoshimori T, Levine B. Methods in Mammalian Autophagy Research.
713 Cell. 2010;140: 313–326.
714 74. Mauvezin C, Neufeld TP. Bafilomycin A1 disrupts autophagic flux by inhibiting both V-
715 ATPase-dependent acidification and Ca-P60A/SERCA-dependent autophagosome-
716 lysosome fusion. Autophagy. 2015;11: 1437–1438.
717 75. Katayama H, Yamamoto A, Mizushima N, Yoshimori T, Miyawaki A. GFP-like proteins
718 stably accumulate in lysosomes. Cell Struct Funct. 2008;33: 1–12.
719 76. Thoreen CC, Kang SA, Won Chang J, Liu Q, Zhang J, Gao Y, et al. An ATP-competitive
720 Mammalian Target of Rapamycin Inhibitor Reveals Rapamycin-resistant Functions of
721 mTORC1. J Biol Chem. 2009;284: 8023–8032.
722 77. Hardy SD, Shinde A, Wang W-H, Wendt MK, Geahlen RL. Regulation of epithelial-
723 mesenchymal transition and metastasis by TGF-β, P-bodies, and autophagy. Oncotarget.

724 2017;8: 103302–103314.
725 78. Liu Q, Xu C, Kirubakaran S, Zhang X, Hur W, Liu Y, et al. Characterization of Torin2, an
726 ATP-competitive inhibitor of mTOR, ATM, and ATR. Cancer Res. 2013;73:2574–2586.
727 79. Kuang E, Tang Q, Maul GG, Zhu F. Activation of p90 Ribosomal S6 Kinase by ORF45 of
728 Kaposi's Sarcoma-Associated Herpesvirus and Its Role in Viral Lytic Replication. J Virol.
729 2008;82: 1838-1850.
730 80. Kayyali US, Pennella CM, Trujillo C, Villa O, Gaestel M, Hassoun PM. Cytoskeletal
731 changes in hypoxic pulmonary endothelial cells are dependent on MAPK-activated protein
732 kinase MK2. J Biol Chem. 2002;277: 42596–42602.
733 81. Rousseau S, Houle F, Landry J, Huot J. P38 MAP kinase activation by vascular
734 endothelial growth factor mediates actin reorganization and cell migration in human
735 endothelial cells. Oncogene. 1997;15: 2169–2177.
736 82. Engel K, Schultz H, Martin F, Kotlyarov A, Plath K, Hahn M, et al. Constitutive
737 activation of mitogen-activated protein kinase-activated protein kinase 2 by mutation of
738 phosphorylation sites and an A-helix motif. J Biol Chem. 1995;270: 27213–27221.
739 83. Guo L, Louis IV-S, Bohjanen PR. Post-transcriptional regulation of cytokine expression
740 and signaling. Curr Trends Immunol. 2018;19: 33–40.
741 84. Franks TM, Lykke-Andersen J. The control of mRNA decapping and P-body formation.
742 Mol Cell. 2008;32: 605–615.
743 85. Ayache J, Bénard M, Ernoult-Lange M, Minshall N, Standart N, Kress M, et al. P-body
744 assembly requires DDX6 repression complexes rather than decay or Ataxin2/2L
745 complexes. Mol Biol Cell. 2015;26: 2579–2595.
746 86. Guo H, Chitiprolu M, Gagnon D, Meng L, Perez-Iratxeta C, Lagace D, et al. Autophagy

747 supports genomic stability by degrading retrotransposon RNA. Nat Commun. 2014;5:
748 5276.
749 87. Kleer M, MacNeil G, Pringle ES, Corcoran JA. A panel of KSHV mutants in the
750 polycistronic kaposin locus for precise analysis of individual protein products. bioRxiv.
751 2021 Jan 1;2021.06.11.448153. Available from:
752 http://biorxiv.org/content/early/2021/09/07/2021.06.11.448153.abstract
753 88. Buchan JR, Kolaitis R, Taylor JP, Parker R. Eukaryotic Stress Granules Are Cleared by
754 Autophagy and Cdc48 / VCP Function. Cell. 2013;153: 1461–1474.
755 89. Turakhiya A, Meyer SR, Marincola G, Böhm S, Vanselow JT, Schlosser A, et al.
756 ZFAND1 Recruits p97 and the 26S Proteasome to Promote the Clearance of Arsenite-
757 Induced Stress Granules. Mol Cell. 2018;70: 906-919.
758 90. Dougherty JD, White JP, Lloyd RE. Poliovirus-mediated disruption of cytoplasmic
759 processing bodies. J Virol. 2011;85: 64–75.
760 91. Bish R, Cuevas-Polo N, Cheng Z, Hambardzumyan D, Munschauer M, Landthaler M, et
761 al. Comprehensive Protein Interactome Analysis of a Key RNA Helicase: Detection of
762 Novel Stress Granule Proteins. Biomolecules. 2015;5: 1441–1466.
763 92. Gustafson EA, Wessel GM. DEAD-box helicases: posttranslational regulation and
764 function. Biochem Biophys Res Commun. 2010;395: 1–6.
765 93. Rahman H, Qasim M, Oellerich M, Asif AR. Crosstalk between Edc4 and mammalian
766 target of rapamycin complex 1 (mTORC1) signaling in mRNA decapping. Int J Mol Sci.
767 2014;15: 23179–23195.
768 94. Yoon J-H, Choi E-J, Parker R. Dcp2 phosphorylation by Ste20 modulates stress granule
769 assembly and mRNA decay in Saccharomyces cerevisiae. J Cell Biol. 2010;189: 813–827.

770 95. Tenekeci U, Poppe M, Beuerlein K, Busch J, Schmitz ML, Kracht M. K63-Ubiquitylation
771 and TRAF6 Pathways Regulate Mammalian P-Body Formation and mRNA Decapping.
772 Mol Cell. 2016;62: 943–57.
773 96. Aizer A, Kafri P, Kalo A, Shav-Tal Y. The P Body Protein Dcp1a Is Hyper-
774 phosphorylated during Mitosis. Prigent C, editor. PLoS One. 2013;8: e49783.
775 97. Chiang PY, Shen YF, Su YL, Kao CH, Lin NY, Hsu PH, et al. Phosphorylation of mRNA
776 Decapping Protein Dcp1a by the ERK Signaling Pathway during Early Differentiation of
777 3T3-L1 Preadipocytes. PLoS One. 2013;8: e61697.
778 98. Vescovo T, Pagni B, Piacentini M, Fimia GM, Antonioli M. Regulation of Autophagy in
779 Cells Infected With Oncogenic Human Viruses and Its Impact on Cancer Development.
780 Front Cell Dev Biol. 2020;8: 47.
781 99. Liu J, Debnath J. The Evolving, Multifaceted Roles of Autophagy in Cancer. Adv Cancer
782 Res. 2016;130: 1–53.
783 100. Pringle ES, Robinson C-A, McCormick C. Kaposi's Sarcoma-Associated Herpesvirus
784 Lytic Replication Interferes with mTORC1 Regulation of Autophagy and Viral Protein
785 Synthesis. J Virol. 2019;93: e00854-19.
786 101. Wu WKK, Coffelt SB, Cho CH, Wang XJ, Lee CW, Chan FKL, et al. The autophagic
787 paradox in cancer therapy. Oncogene. 2012;31: 939–953.
788 102. Kuma A, Hatano M, Matsui M, Yamamoto A, Nakaya H, Yoshimori T, et al. The role of
789 autophagy during the early neonatal starvation period. Nature. 2004;432:1032–1036.
790 103. Myoung J, Ganem D. Generation of a doxycycline-inducible KSHV producer cell line of
791 endothelial origin: maintenance of tight latency with efficient reactivation upon induction.
792 J Virol Methods. 2011;174: 12–21.

793 104. Johnston BP, Pringle ES, McCormick C. KSHV activates unfolded protein response
794 sensors but suppresses downstream transcriptional responses to support lytic replication.
795 PLoS Pathog. 2019;15: e1008185.
796 105. Yoo SM, Ahn AK, Seo T, Hong HB, Chung MA, Jung SD, et al. Centrifugal enhancement
797 of Kaposi's sarcoma-associated virus infection of human endothelial cells in vitro. J Virol
798 Methods. 2008;154: 160-166.
799 106. Castle EL, Douglas P, Rinker KD, Corcoran JA. Viral manipulation of a novel
800 mechanoresponsive signaling axis disassembles processing bodies. bioRxiv.
801 2020;2020.05.15.091876. Available from:
802 http://biorxiv.org/content/early/2020/05/16/2020.05.15.091876.abstract
803 107. Moffat J, Grueneberg DA, Yang X, Kim SY, Kloepfer AM, Hinkle G, et al. A Lentiviral
804 RNAi Library for Human and Mouse Genes Applied to an Arrayed Viral High-Content
805 Screen. Cell. 2006;124: 1283–1298.
806 108. Bryant DM, Datta A, Rodríguez-Fraticelli AE, PeräCurrency Signnen J, Martín-Belmonte
807 F, Mostov KE. A molecular network for de novo generation of the apical surface and
808 lumen. Nat Cell Biol. 2010;12: 1035–1045.
809

810 **Figure Legends**

811 **Figure 1: Kaposin B requires canonical autophagy to disassemble PBs.** Primary human
812 umbilical vein endothelial cells (HUVECs) were transduced with recombinant lentiviruses
813 expressing either Kaposin B (KapB) or an empty vector control and selected with blasticidin (5
814 µg/mL). A: Cells were treated with bafilomycin A1 (10 nM) or a vehicle control (DMSO) for
815 the indicated times prior to harvest in 2x Laemmli buffer. Protein lysates were resolved by SDS-
816 PAGE and immunoblot was performed for p62 and LC3. Samples were quantified using Image
817 Lab (Biorad) software and then normalized, first to total protein and then to their respective
818 starting time points (0 h). Results were plotted in GraphPad and a linear regression statistical
819 test was performed, ±SEM; n=3, *=P<0.05, ***=P<0.001. B: Cells were treated with BafA1 for
820 30 min prior to fixation in methanol. Immunofluorescence was performed for LC3 (white) and
821 DAPI (nuclei, blue). Scale bar=20 µm. Total LC3 area per field was quantified by identifying
822 LC3-positive puncta using CellProfiler and normalizing to the number of nuclei and the vector
823 DMSO control. Results were plotted in GraphPad, a 2-way ANOVA was performed with a
824 Šidák's multiple comparison test, ±SEM; n=3, *=P<0.05. C: HUVECs were sequentially
825 transduced: first with recombinant lentiviruses expressing either shRNAs targeting Atg5 or
826 Atg14 (shAtg5, shAtg14) or a non-targeting control (NS) and selected with puromycin (1
827 µg/mL), and second with either KapB or an empty vector control and selected with blasticidin (5
828 µg/mL). Coverslips were fixed in 4% paraformaldehyde, permeabilized in 0.1% Triton X-100,
829 and immunostained for the PB-resident protein Hedls (white) and nuclei (DAPI). Scale bar=20
830 µm. Hedls puncta were quantified using CellProfiler and normalized to the number of nuclei,
831 results were plotted in GraphPad and a 2-way ANOVA was performed with a Šidák's multiple
832 comparison test, ±SEM; n=3, *=P<0.05. D: HUVECs were transduced as in A and treated with

833 DMSO or bafilomycin A1 (10 nM) for 30 min before being fixed in 4% paraformaldehyde and
834 permeabilized in 0.1% Triton X-100. Immunofluorescence was performed for Hedls (PBs,
835 white) and DAPI (nuclei, blue). Scale bar=20 µm. Hedls puncta were counted using CellProfiler
836 and normalized to the number of nuclei, results were plotted in GraphPad and a 2-way ANOVA
837 was performed with a Šidák's multiple comparison test, ±SEM; n=3, *=P<0.05.
838
839 **Figure 2: Torin treatment disassembles PBs.** A: HUVECs were treated with either Torin (250
840 nM) or a DMSO control for 2 h prior to fixation in 4% paraformaldehyde. Samples were
841 permeabilized in 0.1% Triton X-100. Immunofluorescence was performed for Hedls (PBs,
842 white) and DAPI (nuclei, blue). Scale bar=20 µm. Hedls puncta were counted using CellProfiler
843 and normalized to the number of nuclei, results were plotted in GraphPad and a 2-way ANOVA
844 was performed with a Šidák's multiple comparison test, ±SEM; n=3, *=P<0.05. B: HUVECs
845 were treated with either Torin (250 nM) or a DMSO control for 90 min prior to the addition of
846 sodium arsenite (0.25 mM) for 30 min. Cells were fixed in 4% paraformaldehyde and
847 permeabilized in 0.1% Triton X-100. Immunofluorescence was performed for Hedls (PBs,
848 white) and DAPI (nuclei, blue). Scale bar=20 µm. C: HUVECs were transduced with
849 recombinant lentiviruses expressing either KapB, constitutively active MK2 (MK2EE), or an
850 empty vector control and selected with blasticidin (5 µg/mL). Cells were treated with either
851 Torin (250 nM) or a DMSO control for 2 h prior to harvest in 2x Laemmli buffer. Protein lysates
852 were resolved by SDS-PAGE and immunoblot was performed for phospho-S6 (Ser235/236) and
853 total S6. D: HUVECs were transduced as in C and harvested in 2X Laemmli buffer. Protein
854 lysates were resolved by SDS-PAGE and immunoblot was performed for phospho-Beclin
855 (Ser90) and total Beclin.

856 **Figure 3: KapB-mediated ARE-mRNA reporter expression requires canonical autophagy.**
857 A: HUVECs were transduced with recombinant lentiviruses expressing either KapB or an empty
858 vector control and selected with blasticidin (5 µg/mL). Conditioned media harvested from
859 KSHV latently infected cells was used to mimic the KS lesion microenvironment and induce the
860 transcription of cytokines for 6 h prior to lysis for total RNA, normal media was used for the 0 h
861 time point. Transcript levels were quantified by qPCR and normalized to 18S as a reference
862 gene. Data is represented as the fold change in target transcript expression relative to the
863 untreated vector control and was quantified using the ΔΔCq method. Results were plotted in
864 GraphPad, a 2-way ANOVA was performed, ±SEM; n=3, *=P<0.05, **=P<0.01. B: HUVECs
865 were treated with Torin (250 nM) or a DMSO control for 2 h prior to lysis for total RNA.
866 Transcript levels were quantified by qPCR and normalized to HPRT as a reference gene. Data is
867 represented as the fold change in target transcript expression relative to the untreated vector
868 control and was quantified using the ΔΔCq method. An unpaired t-test was performed, ±SEM;
869 n=3, *=P<0.05. C: HeLa Tet-Off cells were co-transfected with expression plasmids for an
870 ARE-containing firefly luciferase plasmid (pTRE-Fluc-ARE) and a stable renilla luciferase
871 plasmid (pTRE-Rluc). 36 h post transfection, doxycycline (Dox) was added to halt reporter gene
872 transcription of both luciferase reporters, at the same time Torin (250 nM) or DMSO were added;
873 12 h after Dox addition, lysates were harvested in passive lysis buffer (Promega). Luciferase
874 activity for both firefly and renilla was analyzed using the Dual-Luciferase Reporter Assay
875 (Promega) and normalized (firefly/renilla) relative luciferase was calculated in relative light units
876 (RLUs). Results were plotted using GraphPad, an unpaired t-test was performed, ±SEM; n=6,
877 ***=P<0.001. D&E: HeLa Tet-Off cells were transduced with recombinant lentiviruses
878 expressing either shRNAs targeting Atg5 or Atg14 (shAtg5, shAtg14) or a non-targeting control

879 (NS) and selected with puromycin (1 µg/mL). After selection, cells were co-transfected and Dox
880 treatment was performed as described in C, except that co-transfection also included an
881 expression plasmid for KapB or an empty vector control. Results were plotted using GraphPad,
882 an unpaired t-test was performed, ±SEM; n=3, *=P<0.05, **=P<0.01. F: Cells were co-
883 transfected as in E and bafilomycin (10 nM) was added at the same time as Dox. Results were
884 plotted in GraphPad and a Student's t-test was performed, ±SEM; n=3, *=P<0.05, **=P<0.01.
885
886 **Figure 4: Dcp1a protein levels are decreased by KapB expression and Torin treatment.** A:
887 HUVECs were treated with DMSO or Torin (250 nM) for 4 h prior to harvest. Samples were
888 lysed in 2x Laemmli buffer and resolved by SDS-PAGE before immunoblotting with Xrn1,
889 EDC4/Hedls, Dcp1a, and DDX6. Samples were quantified by normalizing the PB resident
890 protein levels to the total protein in each lane and then the DMSO control using ImageLab
891 (Biorad). Results were plotted in GraphPad and a one-way ANOVA was performed ±SEM; n=3,
892 **=P<0.01. B: HUVECs were transduced with recombinant lentiviruses expressing either KapB
893 or an empty vector control and selected with blasticidin (5 µg/mL). Cells were treated with
894 DMSO or bafilomycin A1 (BafA1, 10 nM) for 4 h prior to harvest in 2x Laemmli buffer.
895 Samples were resolved by SDS-PAGE and immunoblot was performed for Dcp1a or p62
896 (autophagy marker). Representative blot is from the same membrane, hashed line indicates
897 skipped lanes. Samples were quantified by normalizing Dcp1a protein levels to the total protein
898 in each lane using Image Lab (Biorad) and then to the Vector DMSO control. Results were
899 plotted in GraphPad and a 2-way ANOVA was performed, ±SEM; n=3, ***=P<0.001. C:
900 HUVECs were transduced with recombinant lentiviruses expressing either KapB or an empty
901 vector control and selected with blasticidin (5 µg/mL). Samples were harvested in 2x Laemmli

902 buffer, resolved by SDS-PAGE and immunoblot was performed for Xrn1, Hedls/EDC4, or
903 DDX6. Samples were quantified by normalizing Dcp1a protein levels to the total protein in each
904 lane using Image Lab (Biorad) and then to the Vector DMSO control. Results were plotted in
905 GraphPad. D: HUVECs were sequentially transduced: first with recombinant lentiviruses
906 expressing either shRNAs targeting Atg5 (shAtg5) or a non-targeting control (NS) and selected
907 with puromycin (1 µg/mL), and second with either KapB or an empty vector control and selected
908 with blasticidin (5 µg/mL). Samples were harvested in 2x Laemmli buffer and resolved by SDS-
909 PAGE. Immunoblot was performed for Dcp1a, Atg5, and KapB. Samples were quantified by
910 normalizing Dcp1a protein levels to the total protein in each lange using Image Lab (Biorad) and
911 then to the Vector NS control. Results were plotted in GraphPad and a 2-way ANOVA was
912 performed, ±SEM; n=3, *=P<0.05, **P=<0.01.
913
914 **Figure 5: KapB-mediated PB disassembly and ARE-mRNA reporter expression require the**
915 **selective autophagy receptor NDP52**. A: HUVECs were sequentially transduced with
916 recombinant lentivirus expressing KapB or an empty vector control and selected with blasticidin
917 (5 µg/mL), and second with shRNAs targeting NDP52, OPTN, p62 or a non-targeting control
918 (NS) and selected with puromycin (1 µg/mL). Coverslips were fixed in 4% paraformaldehyde,
919 permeabilized in 0.1% Triton X-100 and immunostained for Hedls (PBs; white), DAPI (nuclei,
920 blue). Scale bar=20 µm. Cells were imaged and the mean number of Hedls puncta per cell were
921 quantified using CellProfiler. Data were plotted in GraphPad as the mean number of Hedls
922 puncta per cell per condition ± SEM; n=3. A 2-way ANOVA was performed with a Šidák's
923 multiple comparison test; * = P<0.05 **= P<0.01. B: HUVECs were transduced with
924 recombinant lentivirus expressing an shRNA targeting NDP52 and selected with puromycin (1

925 µg/mL). Cells were treated with Torin (250 nM) or a DMSO control for 2 h prior to fixation in
926 4% paraformaldehyde and permeabilization in 0.1% Triton X-100. Samples were
927 immunostained for Hedls (PBs; white), DAPI (nuclei, blue). Scale bar=20 µm. Cells were
928 imaged and the mean number of Hedls puncta per cell were quantified using CellProfiler. Data
929 were plotted in GraphPad as the mean number of Hedls puncta per cell per condition. Results
930 were plotted in GraphPad, a 2-way ANOVA was performed with a Šidák's multiple comparison
931 test, ± SEM; n=3. * = P<0.05. C: HeLa Tet-Off cells were transduced with recombinant
932 lentivirus expressing shRNAs targeting NDP52, OPTN, p62 or a NS control and selected with
933 puromycin (1µg/mL) then cells were co-transfected, treated with Dox and luciferase activity was
934 recorded and analyzed as in Figure 3. Data were plotted in GraphPad as the mean fold change in
935 the relative luciferase activity of each condition compared to vector NS or KapB NS; n=3. An
936 unpaired t-test was performed; * = P<0.05 **= P<0.01. D: HUVECs were sequentially
937 transduced first with recombinant lentivirus expressing shDNP52 targeting the 3'-UTR of
938 NDP52 or a NS control and selected with blasticidin (5 µg/mL), and second, with KapB and
939 either mCherry control (mCh) or RFP-NDP52. Coverslips were fixed with 4%
940 paraformaldehyde, permeabilized with 0.1% Triton X-100, and immunostained with Hedls (PBs,
941 green). Scale bar=20 µm. E: Samples from D were quantified; Hedls puncta were counted using
942 CellProfiler and normalized to the number of nuclei, results were plotted in GraphPad, a 2-way
943 ANOVA was performed with a Šidák's multiple comparison test, ± SEM; n=3. * = P<0.05,
944 **=P<0.01.
945
946 **Figure 6: MK2EE-mediated PB disassembly does not require NDP52 or canonical**
947 **autophagy.** A: HUVECs were transduced with recombinant lentiviruses expressing either

948 constitutively active MK2 (MK2EE) or an empty vector control and selected with blasticidin (5
949 µg/mL) for 48 h. Cells were treated with DMSO or bafilomycin A1 (10 nM) for 30 min before
950 being fixed in methanol. Immunofluorescence was performed for LC3 (autophagosomes, white)
951 and DAPI (nuclei, blue). Scale bar=20 µm. Total LC3 area per field was quantified by
952 identifying LC3 puncta using CellProfiler and normalizing to the number of nuclei and the vector
953 DMSO control. Results were plotted in GraphPad and a 2-way ANOVA was performed with a
954 Šidák's multiple comparison test, ±SEM n=3; *=P<0.05. B: HUVECs were transduced with
955 recombinant lentiviruses expressing either MK2EE or an empty vector control and selected with
956 blasticidin (5 µg/mL). Cells were treated with bafilomycin A1 (10 nM) or a vehicle control
957 (DMSO) for the indicated times prior to harvest in 2x Laemmli buffer. Protein lysates were
958 resolved by SDS-PAGE and immunoblot was performed for p62 and LC3. Representative blot
959 is from the same membrane, hashed line indicates skipped lanes. Samples were quantified using
960 Image Lab (Biorad) software and then normalized, first to total protein and then to their
961 respective starting points (time 0 h). Results were plotted in GraphPad and a linear regression
962 statistical test was performed, ±SEM; n=3, *=P<0.05, **=P<0.01. C: HUVECs were
963 sequentially transduced: first with recombinant lentiviruses expressing either shRNAs targeting
964 Atg5 (shAtg5) or a non-targeting control (NS) and selected with puromycin (1 µg/mL), and
965 second, with either MK2EE or an empty vector control and selected with blasticidin (5 µg/mL).
966 Coverslips were fixed in 4% paraformaldehyde, permeabilized in 0.1% Triton X-100, and
967 immunostained for the PB-resident protein Hedls (PBs, white) and DAPI (nuclei, blue). Scale
968 bar=20 µm. Hedls puncta were counted using CellProfiler and normalized to the number of
969 nuclei, results were plotted in GraphPad and a 2-way ANOVA was performed with a Šidák's
970 multiple comparison test, ±SEM n=5; *=P<0.05. D: HeLa Tet-Off cells were transduced with

971 recombinant lentiviruses expressing either shRNAs targeting Atg5 (shAtg5) or a non-targeting
972 control (NS) and selected with puromycin (1 µg/mL) then co-transfected with expression
973 plasmids for pTRE-Fluc-ARE, pTRE-Rluc, and MK2EE or an empty vector control, and treated
974 as in Figure 3. Results were plotted using GraphPad, a Student's t-test was performed, ±SEM,
975 n=4; *=P<0.05. E: HUVECs were sequentially transduced with recombinant lentivirus
976 expressing shRNAs targeting NDP52, OPTN, p62 or a non-targeting control (NS) and selected
977 with puromycin (1 µg/mL) and second with recombinant lentivirus expressing constitutively
978 active MK2EE or an empty vector control and selected with blasticidin (5 µg/mL). Coverslips
979 were fixed in 4% v/v paraformaldehyde, permeabilized in 0.1% Triton X-100, and
980 immunostained for Hedls (PBs, white) and DAPI (nuclei, blue). Scale bar = 20 µm. Hedls puncta
981 were counted using CellProfiler and normalized to the number of nuclei, results were plotted in
982 GraphPad, ±SEM; n=3. F: HeLa Tet-Off cells were transduced with recombinant lentivirus
983 expressing shRNAs targeting NDP52, OPTN, p62 or a NS control and selected with puromycin
984 (1µg/mL) then cells were co-transfected, treated with Dox and luciferase activity was recorded
985 and analyzed as in Figure 3. Data were plotted in GraphPad as the mean fold change in the
986 relative luciferase activity of each condition compared to vector NS or MK2EE NS; n=3. An
987 unpaired t-test was performed; * = P<0.05 **= P<0.01.
988
989 **Figure 7: KSHV-mediated PB disassembly requires Atg5 and the selective autophagy**
990 **receptor NDP52.** A: HUVECs were infected with rKSHV.219 via spinoculation and infection
991 was allowed to proceed for 96 h prior to treatment with bafilomycin A1 (10 nM) for 30 min.
992 Coverslips were fixed in 4% paraformaldehyde, permeabilized in 0.1% Triton X-100 and
993 immunostained for Hedls (PBs; white), LANA (KSHV latency, green), and DAPI (nuclei, blue).

994 Scale bar=20 µm. Cells were imaged and the mean number of Hedls puncta per cell were
995 quantified using CellProfiler. Data were plotted in GraphPad as the mean number of Hedls
996 puncta per cell ± SEM; n=3. A 2-way ANOVA was performed with a Šidák's multiple
997 comparison test; * = P<0.05. B: HUVECs were transduced with recombinant lentivirus
998 expressing shRNAs targeting Atg5, NDP52, or a non-targeting control (NS) and selected with
999 puromycin (1 µg/mL). Cells were infected with rKSHV.219 via spinoculation and infection was
1000 allowed to proceed for 96 h. Coverslips were fixed in 4% paraformaldehyde, permeabilized in
1001 0.1% Triton X-100 and immunostained for Hedls (PBs; white), LANA (KSHV latency, green),
1002 and DAPI (nuclei, blue). Scale bar=20 µm. Cells were imaged and the mean number of Hedls
1003 puncta per cell were quantified using CellProfiler. Data were plotted in GraphPad as the mean
1004 number of Hedls puncta per cell ± SEM; n=3. A 2-way ANOVA was performed with a Šidák's
1005 multiple comparison test; * = P<0.05. C: HUVECs were transduced with recombinant
1006 lentiviruses and infected with rKSHV.219 as in B. Cells were harvested in 2X Laemmli buffer.
1007 Protein lysates were resolved by SDS-PAGE and immunoblot was performed for Atg5 and
1008 NDP52.
1009
1010 **Tables**
1011 Table 1: Drugs

Drug	Vendor/Catalogue #	Concentration
Torin1	Sigma-Aldrich 475991	250 nM
Bafilomycin A1	Sigma-Aldrich B1793	10 nM
Chloroquine	Sigma-Aldrich C6628	25 µM
MG-132	Selleckchem S2619	5 µM
LPS	Sigma-Aldrich L3129	1 µg/mL
Sodium Arsenite	Sigma-Aldrich 1.06277	0.25 mM
Doxycycline	Sigma-Aldrich D9891	1 µg/mL

1012
1013 Table 2: Plasmids

Plasmid	Use	Source	Mammalian Selection
RFP-NDP52	Overexpression	Dr. Andreas Till (University Hospital of Bonn)	N/A
pcDNA 3.1 (+)	Empty Vector Control	Invitrogen V79020	N/A
pcDNA KapB BCBL1	ARE-mRNA stability	(51)	N/A
pcDNA FLAG-MK2EE	ARE-mRNA stability	(51)	N/A
pLKO.1-TRC	shRNA expression	Addgene #10878 (107)	Puromycin
pLKO.1-blast	shRNA expression	Addgene #26655 (108)	Blasticidin
pLJM1	Empty Vector Control	(104)	Blasticidin/ Puromycin
pLJM1 KapB (pulmonary KS)	Overexpression	Cloned from pBMNIP-KapB (51) into pLJM1-BSD	Blasticidin
pLJM1 mCh	Overexpression Control	Craig McCormick (Dalhousie University)	Blasticidin
pLJM1 FLAG-MK2EE	Overexpression	Cloned into pLJM1 using BamHI and EcoRI from pBMN FLAG-MK2EE (51)	Blasticidin/ Puromycin
pLJM1 RFP-NDP52	Overexpression	Cloned into pLJM1 using NheI and BamHI from RFP-NDP52	Puromycin
pMD2.G	Lentivirus generation	Addgene #12259	N/A
psPAX2	Lentivirus generation	Addgene #12260	N/A
pTRE2 Firefly Luciferase-ARE	ARE-mRNA stability	(65)	N/A
pTRE2-Renilla Luciferase	ARE-mRNA stability	(65)	N/A

1014

1015 Table 3: shRNA target sequences

shRNA target	shRNA sequence 5'→3'	Region
Non-targeting (NS)	AGCACAAGCTGGAGTACAACTA	
Atg5	CTTTGATAATGAACAGTGAGA	CDS
NDP52(1)	GAGCTGCTTCAACTGAAAGAA	CDS
NDP52(2)	GACTTGCCTATGGAAACCCAT	CDS
NDP52(3)	CCCTTTGTGAACTAAGTTCAA	3'-UTR
NDP52(4)	CCTGACTTGATACTAAGTGAT	3'-UTR
Optineurin (1)	GCACGGCATTGTCTAAATATA	CDS
Optineurin (2)	GCCATGAAGCTAAATAATCAA	CDS
p62	CCGAATCTACATTAAAGAGAA	CDS
NBR1 (1)	GCCAGGAACCAAGTTTATCAA	CDS
NBR1 (2)	CCATCCTACAATATCTGTGAA	CDS
VCP (1)	ACCGTCCCAATCGGTTAATTG	CDS
VCP (2)	AGATCCGTCGAGATCACTTTG	CDS

1016

1017 Table 4: Antibodies

Antibody	Species	Vendor/Catalogue #	Application	Dilution
Hedls	Mouse	Santa Cruz sc-8418	Immunofluorescence Immunoblot	1:1000 1:1000
KapB	Rabbit	A generous gift from Don Ganem	Immunofluorescence	1:1000
NDP52	Rabbit	CST 60732	Immunoblot	1:1000
p62	Rabbit	CST 7695	Immunoblot	1:1000
Dcp1a	Mouse	CST 15365	Immunoblot	1:500
DDX6	Rabbit	Bethyl A300-461	Immunoblot	1:1000
MK2	Rabbit	CST 12155	Immunofluorescence	1:1000
LC3B	Rabbit	CST 2775	Immunofluorescence Immunoblot	1:200 1:1000
Atg5	Rabbit	CST 2630	Immunoblot	1:1000
Atg14	Rabbit	CST 96752	Immunoblot	1:1000
OPTN	Rabbit	Abcam ab23666	Immunoblot	1:1000
Xrn1	Rabbit	Abcam ab231197	Immunoblot	1:1000
VCP	Rabbit	CST 2649	Immunoblot	1:1000
NBR1	Rabbit	CST 9891	Immunoblot	1:1000
LANA	Rabbit	A generous gift from Don Ganem	Immunofluorescence	1:1000
Phospho-S6 (Ser235/236)	Rabbit	CST 4858	Immunoblot	1:1000
Total S6	Rabbit	CST 2217	Immunoblot	1:1000
Phospho-Beclin (Ser90)	Rabbit	CST 86455	Immunoblot	1:500
Total Beclin	Mouse	CST 4122	Immunoblot	1:1000

1018

1019 Table 5: qPCR primers

Primer	Primer Sequence
HPRT-1- Forward	5’ CTTTCCTTGGTCAGGCAGTATAA 3’
HPRT-2 - Reverse	5’ AGTCTGGCTTATATCCAACACTTC 3’
18S - Forward	5’ TTCGAACGTCTGCCCTATCAA 3’
18S - Reverse	5’ GATGTGGTAGCCGTTTCTCAGG 3’
IL-6 - Forward	5’ GAAGCTCTATCTCGCCTCCA 3’
IL-6 - Reverse	5’ TTTTCTGCCAGTGCCTCTTT 3’
CXCL8 - Forward	5’ AAATCTGGCAACCCTAGTCTG 3’
CXCL8 - Reverse	5’ GTGAGGTAAGATGGTGGCTAAT 3’
IL-1β - Forward	5’ CTCTCACCTCTCCTACTCACTT 3’
IL-1β - Reverse	5’ TCAGAATGTGGGAGCGAATG 3’
COX-2 - Forward	5’ CCCTTGGGTGTCAAAGGTAA 3’
COX-2 - Reverse	5’ GCCCTCGCTTATGATCTGTC 3’

1020

1021 **Supplemental Figure Legends**

1022 **Figure S1: KapB expression promotes PB disassembly but does not prevent PB assembly.**
1023 HeLa cells expressing a doxycycline-inducible GFP-Dcp1a were used to determine whether
1024 KapB prevented granule assembly or promoted disassembly. A: HeLa cells were transfected
1025 with either KapB or an empty vector control prior to inducing expression of GFP-Dcp1a with
1026 doxycycline (1 µg/mL). Cells were fixed 12 h post-induction and immunostained for Hedls
1027 (PBs, red) and KapB (blue). Scale bar=20 µm. B: GFP-Dcp1a expression was induced with
1028 doxycycline (1 µg/mL) in HeLa cells prior to transfection with either KapB or an empty vector
1029 control. Cells were fixed 12 h post-transfection and immunostained for Hedls (PBs, red) and
1030 KapB (blue). Scale bar=20 µm. C: HUVECs were transduced with recombinant lentiviruses
1031 expressing either Kaposin B (KapB) or an empty vector control and selected with blasticidin (5
1032 µg/mL). Cells were treated with sodium arsenite (0.25 mM) or a vehicle control for 30 min prior
1033 to fixation in 4% paraformaldehyde and permeabilization in 0.1% Triton X-100. Scale bar=20
1034 µm.
1035 **Figure S2: Canonical autophagy knockdown prevents KapB-mediated PB disassembly.**
1036 A&B: HUVECs were sequentially transduced: first with recombinant lentiviruses expressing
1037 either shRNAs targeting Atg5 or Atg14 (shAtg5, shAtg14) or a non-targeting control (NS) and
1038 selected with puromycin (1 µg/mL), and second with either KapB or an empty vector control and
1039 selected with blasticidin (5 µg/mL). Samples were lysed in 2x Laemmli and resolved by SDS-
1040 PAGE. Samples were immunoblotted for Atg5 (A) or Atg14 (B). For Atg5 (A), representative
1041 blot is from the same membrane, hashed line indicates skipped lanes. For Atg5 (A) samples were
1042 quantified by normalizing Atg5 protein levels to the total protein in each lane using Image Lab
1043 (Biorad) and then to Vector NS. Results were plotted in GraphPad, a 2-way ANOVA was
1044 performed, ±SEM; n=3, ***=P<0.001. C: Atg5 +/+ (WT) and -/- (KO) MEFs were transduced as

1045 in A and harvested in 2x Laemmli buffer before being resolved by SDS-PAGE. Samples were
1046 probed for LC3, a representative blot is shown. D: Atg5 +/+ and -/- MEFs were transduced with
1047 recombinant viruses expressing KapB or an empty vector control and selected with blasticidin (5
1048 μg/mL). Samples were fixed in 4% paraformaldehyde and permeabilized in 0.1% Triton X-100.
1049 Immunofluorescence was performed for Hedls (PBs, white) and DAPI (nuclei, blue). Scale
1050 bar=20 μm. Hedls puncta were counted using CellProfiler and normalized to the number of
1051 nuclei, results were plotted in GraphPad and a 2-way ANOVA was performed with a Šidák's
1052 multiple comparison test, ±SEM; n=3, *=P<0.05, **=P<0.01.

1053 **Figure S3: Canonical autophagy shRNA silencing in HeLa cells.** A&B: HeLas were
1054 transduced with recombinant lentiviruses expressing either shRNAs targeting Atg5 or Atg14
1055 (shAtg5, shAtg14) or a non-targeting control (NS) and selected with puromycin (1 μg/mL) prior
1056 to transfection with KapB or an empty vector for luciferase assays. Samples were lysed in 2x
1057 Laemmli buffer and resolved by SDS-PAGE before immunoblotting with Atg5 (A) or Atg14 (B).
1058 Representative blots are shown.

1059 **Figure S4: Selective autophagy receptor knockdown in HUVECs reveals that OPTN and**
1060 **p62 are not required for KapB-mediated PB disassembly.** A&B: HUVECs were transduced
1061 with shRNAs targeting VCP, NBR1, or a non-targeting control (NS) and selected with
1062 puromycin (1 μg/mL), then transduced with an empty vector control or KapB and selected with
1063 blasticidin (5 μg/mL). Samples were lysed in 2x Laemmli buffer, resolved by SDS-PAGE, and
1064 immunoblotted for NBR1 (A) and VCP (B). Representative blots are shown, successful VCP
1065 knockdown was lethal, while NBR1 knockdown was not successful. C: HUVECs were
1066 transduced with shRNAs targeting NDP52 or a non-targeting control (NS) and selected with
1067 puromycin (1 μg/mL), then transduced with an empty vector control or KapB and selected with

1068 blasticidin (5 µg/mL). Samples were lysed in 2x Laemmli buffer, resolved by SDS-PAGE, and
1069 immunoblotted for NDP52. D&E: HUVECs were transduced with shRNAs targeting p62,
1070 OPTN, or a non-targeting control (NS) and selected with puromycin (1 µg/mL), then transduced
1071 with an empty vector control or KapB and selected with blasticidin (5 µg/mL). Samples were
1072 lysed in 2x Laemmli buffer and resolved by SDS-PAGE. Samples were immunoblotted for p62
1073 (D) and OPTN (E), representative blots are shown. F: HUVECs were transduced as in D and E.
1074 Coverslips were fixed in 4% paraformaldehyde, permeabilized in 0.1% Triton X-100 and
1075 immunostained for Hedls (PBs; white), DAPI (nuclei, blue). Scale bar=20 µm. G: HUVECs were
1076 transduced with recombinant lentiviruses targeting NDP52 or a non-targeting control (NS) and
1077 selected with puromycin (1 µg/mL). Samples were lysed in 2x Laemmli buffer, resolved by
1078 SDS-PAGE, and immunoblotted for NDP52 to confirm knockdown for paired Torin
1079 immunofluorescence experiments.
1080 **Figure S5: shRNA silencing of selective autophagy receptors in HeLa cells.** A, B&C: HeLas
1081 were transduced with shRNAs targeting NDP52, OPTN, p62, or a non-targeting control (NS) and
1082 selected with puromycin (1 µg/mL) prior to transfection with KapB or an empty vector for
1083 luciferase assays. Samples were lysed in 2x Laemmli buffer, resolved by SDS-PAGE, and
1084 immunoblotted for NDP52 (A), p62 (B), and OPTN (C). Representative blots are shown.
1085 **Figure S6: NDP52 shRNA silencing and rescue in control HUVECs.** A: Representative
1086 western blot of HUVECs transduced with an shRNA targeting the 3'UTR of NDP52 or a non-
1087 targeting control (NS) and selected with puromycin (1 µg/mL), then co-transduced with an
1088 empty vector control and mCherry (mCh) or KapB and mCh. Samples were lysed in 2x
1089 Laemmli, resolved by SDS-PAGE, and immunoblotted for NDP52. B: HUVECs were
1090 sequentially transduced first with recombinant lentivirus expressing shDNP52 targeting the 3'-

1091 UTR of NDP52 or a NS control and selected with blasticidin (5 µg/mL), and second, with vector
1092 and either an mCherry control (mCh) or RFP-NDP52. Coverslips were fixed with 4% v/v
1093 paraformaldehyde, permeabilized with 0.1% Triton X-100, and were immunostained with Hedls
1094 (PBs, green). Scale bar=20 µm. C: Hedls puncta were counted using CellProfiler and normalized
1095 to the number of nuclei, results were plotted in GraphPad.

1096 **Figure S7: shRNA silencing of canonical and selective autophagy genes in MK2EE-**
1097 **expressing cells.** A: HUVECs were transduced with shRNAs targeting Atg5 or a non-targeting
1098 control (NS) and selected with puromycin (1 µg/mL), then transduced with an empty vector
1099 control or KapB and selected with blasticidin (5 µg/mL). Samples were lysed in 2x Laemmli
1100 buffer, resolved by SDS-PAGE, and immunoblotted for Atg5. A representative blot is shown. B:
1101 HeLas were transduced with recombinant lentiviruses expressing either shRNAs targeting Atg5
1102 or a non-targeting control (NS) and selected with puromycin (1 µg/mL) prior to transfection with
1103 MK2EE or an empty vector for luciferase assays. Samples were lysed in 2x Laemmli buffer and
1104 resolved by SDS-PAGE before immunoblotting for Atg5. A representative blot is shown. C,
1105 D&E: HUVECs were transduced with shRNAs targeting NDP52, p62, OPTN, or a non-targeting
1106 control (NS) and selected with puromycin (1 µg/mL), then transduced with an empty vector
1107 control or MK2EE and selected with blasticidin (5 µg/mL). Samples were lysed in 2x Laemmli
1108 buffer and resolved by SDS-PAGE. Samples were immunoblotted for NDP52 (C), p62 (D), and
1109 OPTN (E), representative blots are shown. F: HUVECs were transduced with shRNAs as in
1110 D&E. Coverslips were fixed, permeabilized, and immunostained for Hedls (PBs; white), DAPI
1111 (nuclei, blue). Scale bar=20 µm. G, H&I: HeLas were transduced with shRNAs targeting
1112 NDP52, OPTN, p62, or a non-targeting control (NS) and selected with puromycin (1 µg/mL),
1113 then transfected with an empty vector control or MK2EE for luciferase assays. Samples were

1114 lysed in 2x Laemmli buffer, resolved by SDS-PAGE, and immunoblotted for NDP52 (G), p62

1115 (H), and OPTN (I). Representative blots are shown.

1116

1117

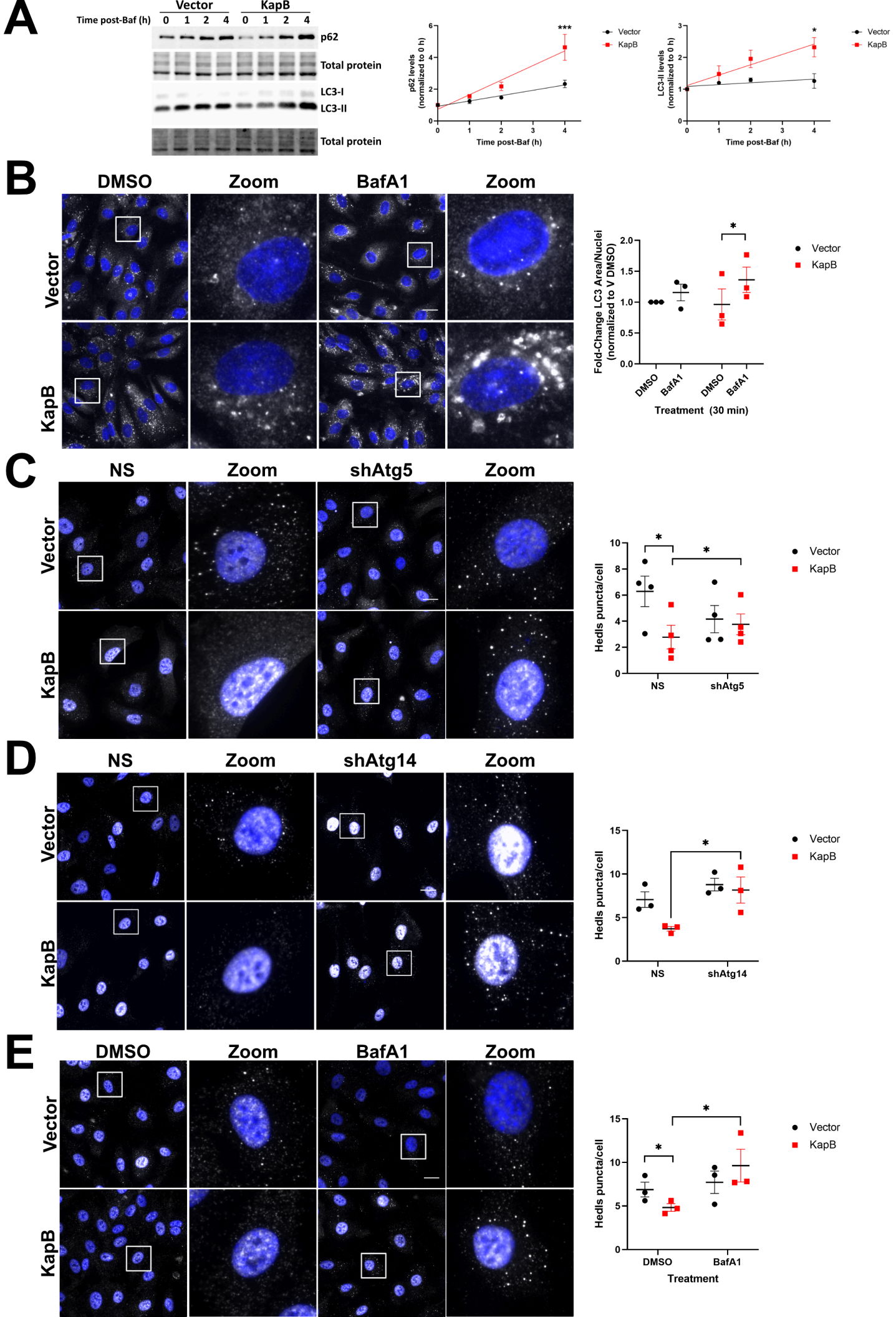
A
Vector
KapB
Time post-Baf (h)
0 1 2 4 0 1 2 4
p62
Total protein
LC3-I
LC3-II
Total protein
p62 levels (normalized to 0 h)
Time post-Baf (h)
***
Vector
KapB
LC3-II levels (normalized to 0 h)
Time post-Baf (h)
*
Vector
KapB
B
DMSO
Zoom
BafA1
Zoom
Vector
KapB
Fold-Change LC3 Area/Nuclei (normalized to V DMSO)
Treatment (30 min)
DMSO
BafA1
DMSO
BafA1
*
Vector
KapB
C
NS
Zoom
shAtg5
Zoom
Vector
KapB
Hedls puncta/cell
NS
shAtg5
*
*
Vector
KapB
D
NS
Zoom
shAtg14
Zoom
Vector
KapB
Hedls puncta/cell
NS
shAtg14
*
Vector
KapB
E
DMSO
Zoom
BafA1
Zoom
Vector
KapB
Hedls puncta/cell
DMSO
BafA1
Treatment
*
*
Vector
KapB

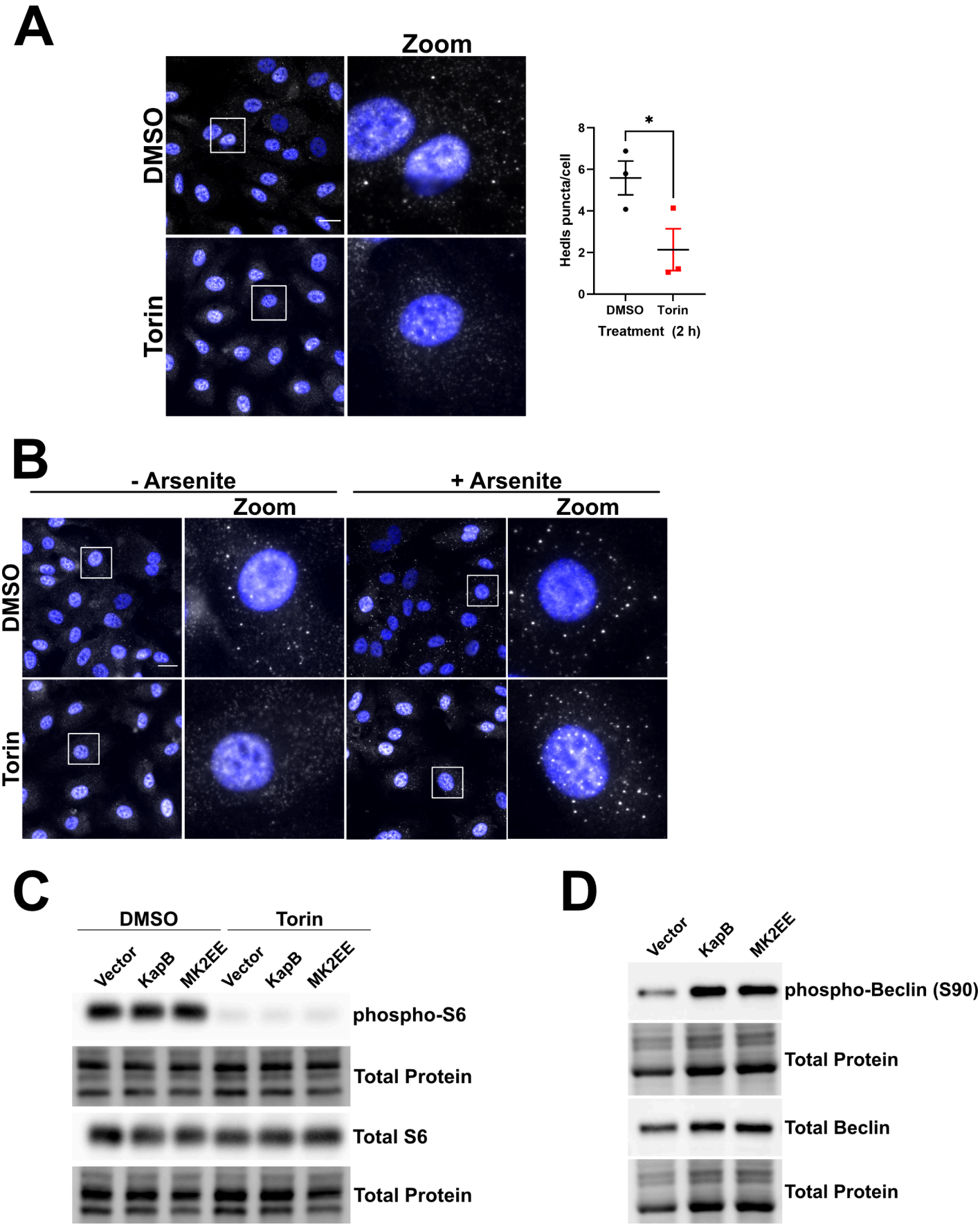
A
Zoom
DMSO
Torin
Hedls puncta/cell
8
6
4
2
0
*
DMSO
Torin
Treatment (2 h)
B
- Arsenite
+ Arsenite
Zoom
Zoom
DMSO
Torin
C
DMSO
Torin
Vector
KapB
MK2EE
Vector
KapB
MK2EE
phospho-S6
Total Protein
Total S6
Total Protein
D
Vector
KapB
MK2EE
phospho-Beclin (S90)
Total Protein
Total Beclin
Total Protein

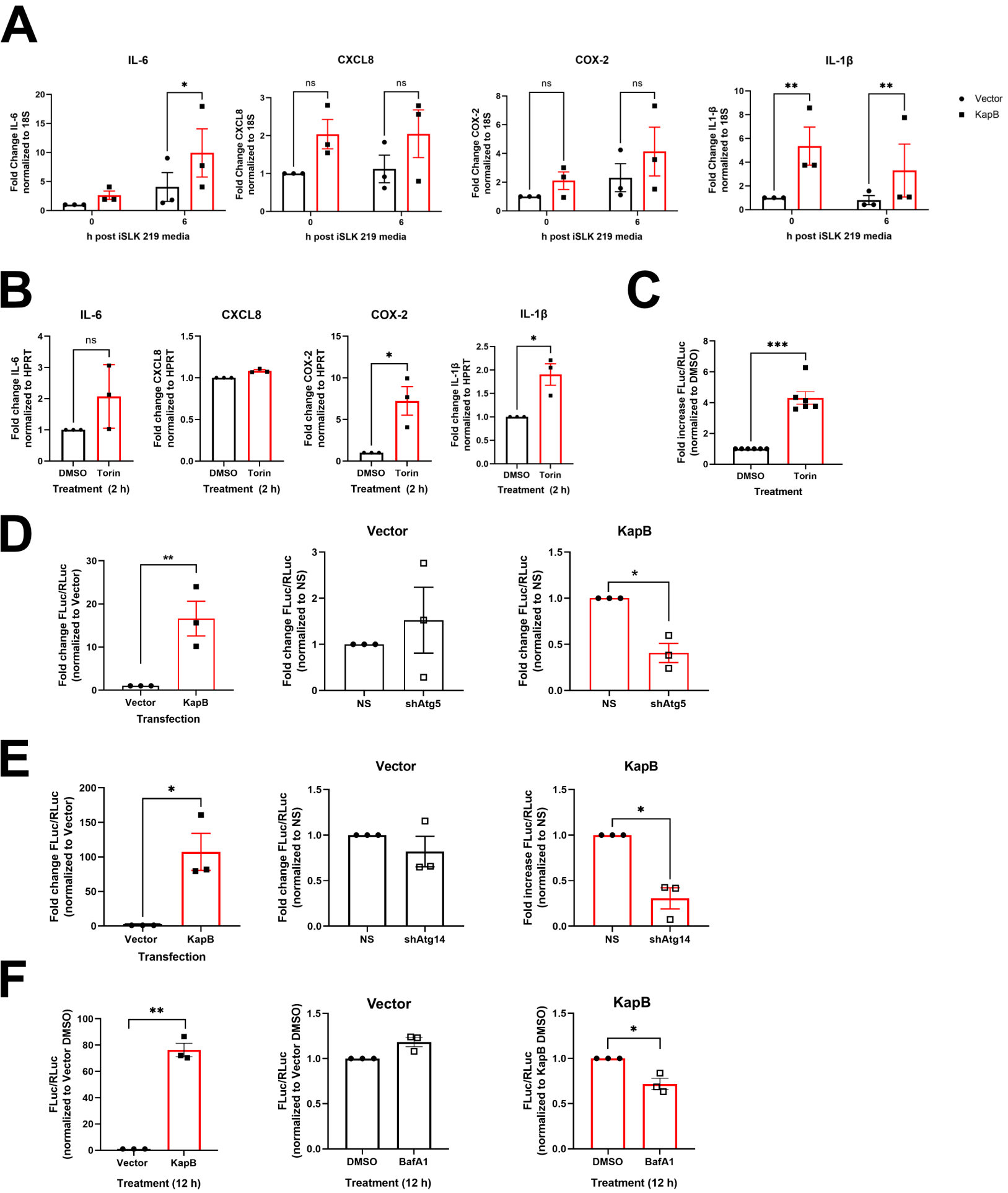
A
IL-6
CXCL8
COX-2
IL-1β
Fold Change IL-6 normalized to 18S
Fold Change CXCL8 normalized to 18S
Fold Change COX-2 normalized to 18S
Fold Change IL1-β normalized to 18S
h post iSLK 219 media
Vector
KapB
B
Fold change IL-6 normalized to HPRT
Fold change CXCL8 normalized to HPRT
Fold change COX-2 normalized to HPRT
Fold change IL-1β normalized to HPRT
DMSO
Torin
Treatment (2 h)
C
Fold increase FLuc/RLuc (normalized to DMSO)
Treatment
D
Fold change FLuc/RLuc (normalized to Vector)
Transfection
Fold change FLuc/RLuc (normalized to NS)
NS
shAtg5
E
Fold increase FLuc/RLuc (normalized to NS)
shAtg14
F
FLuc/RLuc (normalized to Vector DMSO)
FLuc/RLuc (normalized to Vector DMSO)
FLuc/RLuc (normalized to KapB DMSO)
BafA1
Treatment (12 h)

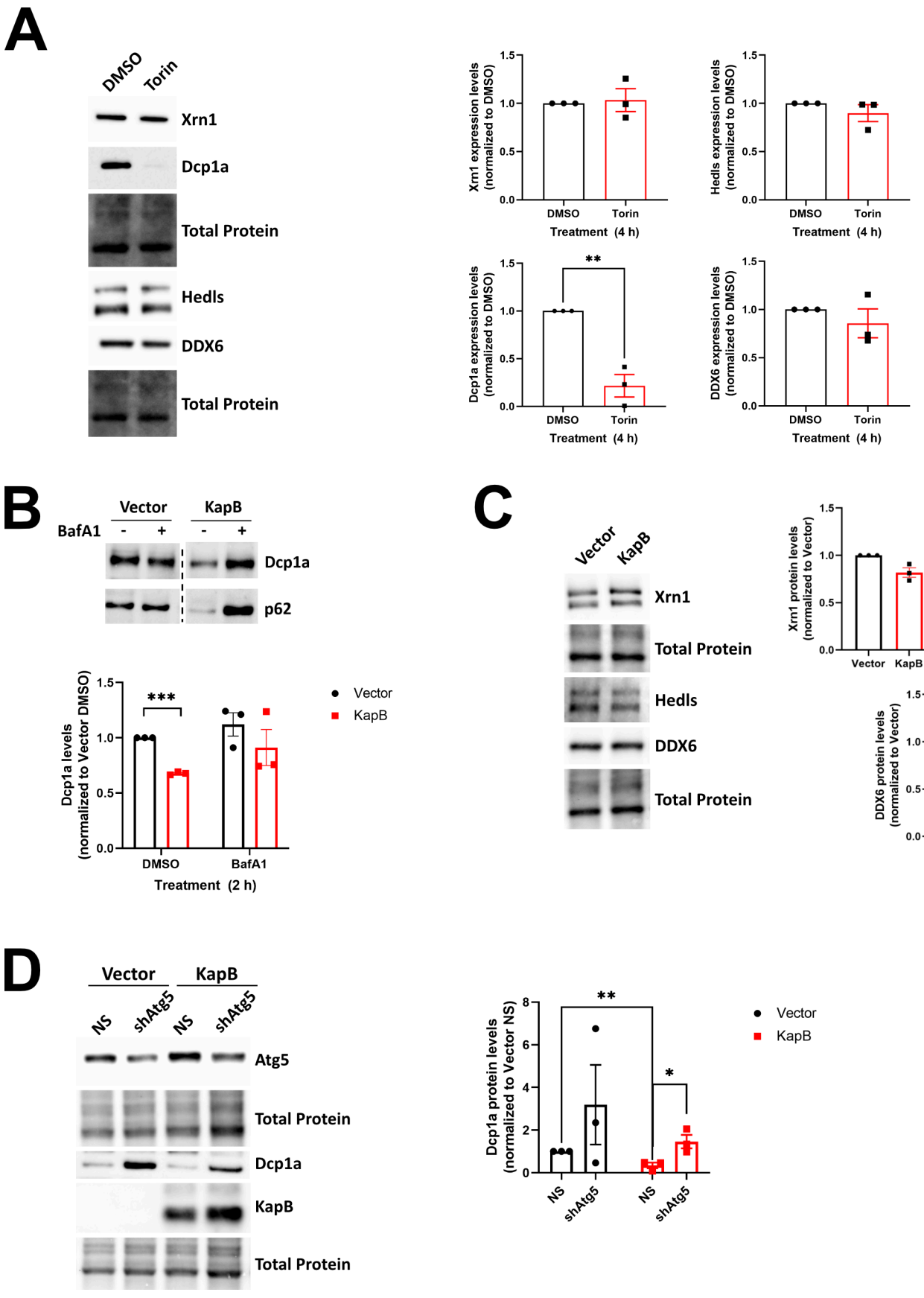
A
DMSO
Torin
Xrn1
Dcp1a
Total Protein
Hedls
DDX6
Total Protein
Xrn1 expression levels (normalized to DMSO)
Hedls expression levels (normalized to DMSO)
Dcp1a expression levels (normalized to DMSO)
DDX6 expression levels (normalized to DMSO)
1.5
1.0
0.5
0.0
**
DMSO
Torin
Treatment (4 h)
B
Vector
KapB
BafA1
-
+
Dcp1a
p62
Dcp1a levels (normalized to Vector DMSO)
***
Vector
KapB
DMSO
BafA1
Treatment (2 h)
C
Vector
KapB
Xrn1
Total Protein
Hedls
DDX6
Total Protein
Xrn1 protein levels (normalized to Vector)
Hedls protein levels (normalized to Vector)
DDX6 protein levels (normalized to Vector)
D
Vector
KapB
NS
shAtg5
Atg5
Total Protein
Dcp1a
KapB
Total Protein
Dcp1a protein levels (normalized to Vector NS)
8
6
4
2
0
**
*

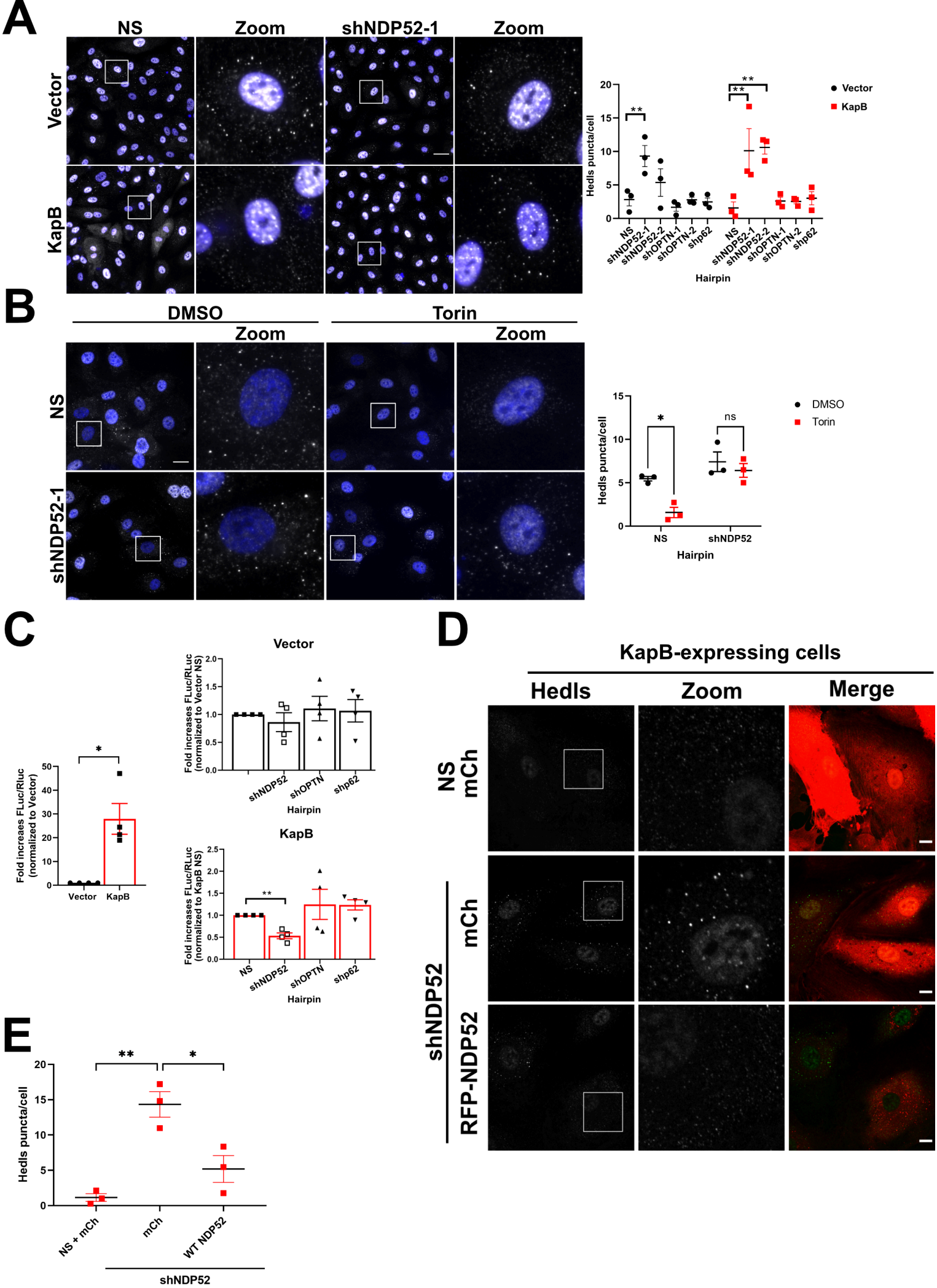
A
NS
Zoom
shNDP52-1
Zoom
Vector
KapB
Hedls puncta/cell
Vector
KapB
NS
shNDP52-1
shNDP52-2
shOPTN-1
shOPTN-2
shp62
Hairpin
B
DMSO
Torin
Zoom
Zoom
NS
shNDP52-1
Hedls puncta/cell
DMSO
Torin
ns
NS
shNDP52
Hairpin
C
Fold increaes FLuc/Rluc (normalized to Vector)
Vector
KapB
Vector
Fold increases FLuc/RLuc (normalized to Vector NS)
shNDP52
shOPTN
shp62
Hairpin
KapB
Fold increases FLuc/RLuc (normalized to KapB NS)
NS
shNDP52
shOPTN
shp62
Hairpin
D
KapB-expressing cells
Hedls
Zoom
Merge
NS mCh
shNDP52
mCh
RFP-NDP52
E
Hedls puncta/cell
NS + mCh
mCh
WT NDP52
shNDP52

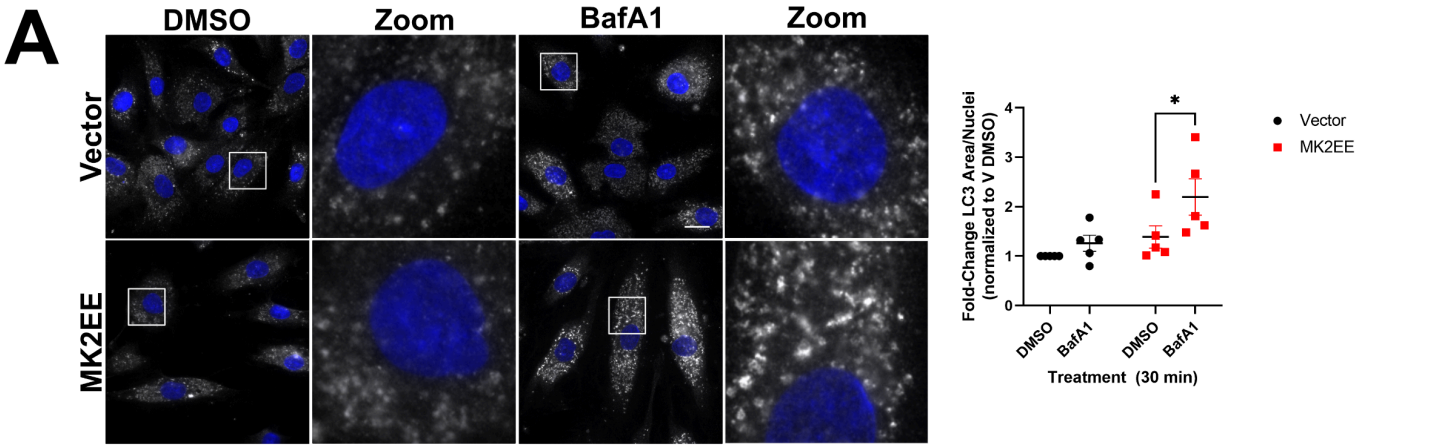
A
DMSO
Zoom
BafA1
Zoom
Vector
MK2EE
Fold-Change LC3 Area/Nuclei (normalized to V DMSO)
Treatment (30 min)
DMSO
BafA1
DMSO
BafA1
Vector
MK2EE

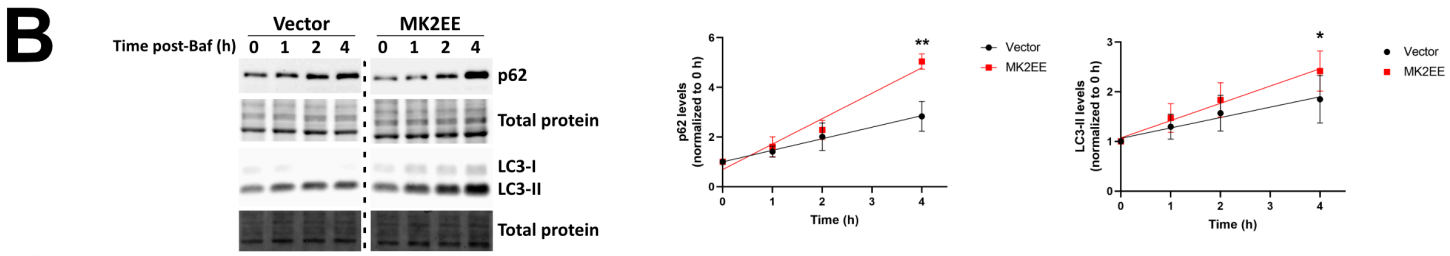
B
Vector
MK2EE
Time post-Baf (h)
0 1 2 4
0 1 2 4
p62
Total protein
LC3-I
LC3-II
Total protein
p62 levels (normalized to 0 h)
Time (h)
LC3-II levels (normalized to 0 h)
Time (h)
Vector
MK2EE

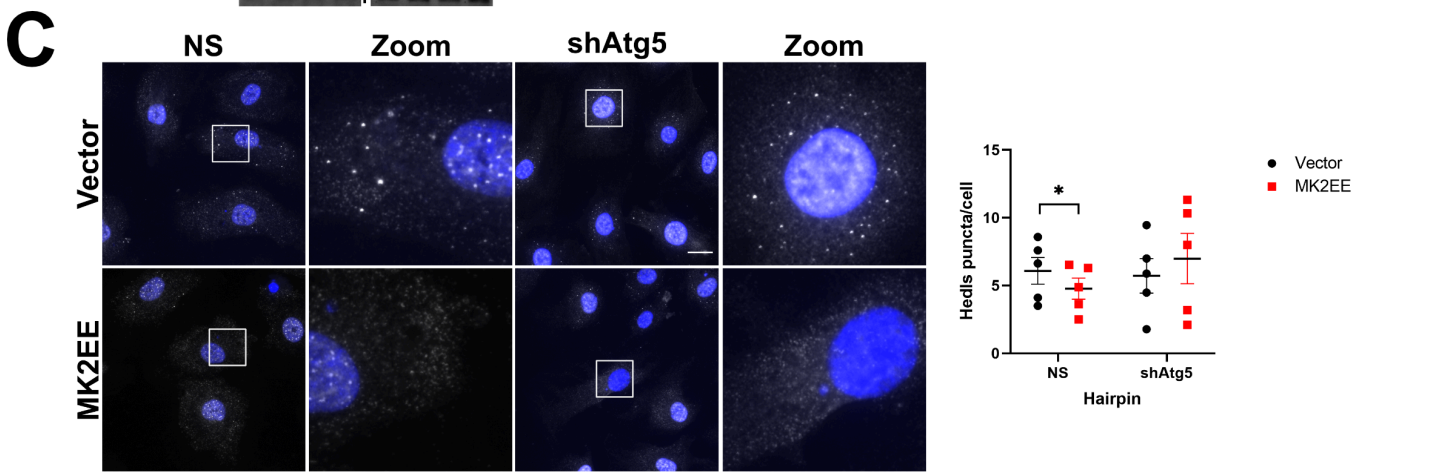
C
NS
Zoom
shAtg5
Zoom
Vector
MK2EE
Hedls puncta/cell
NS
shAtg5
Hairpin
Vector
MK2EE

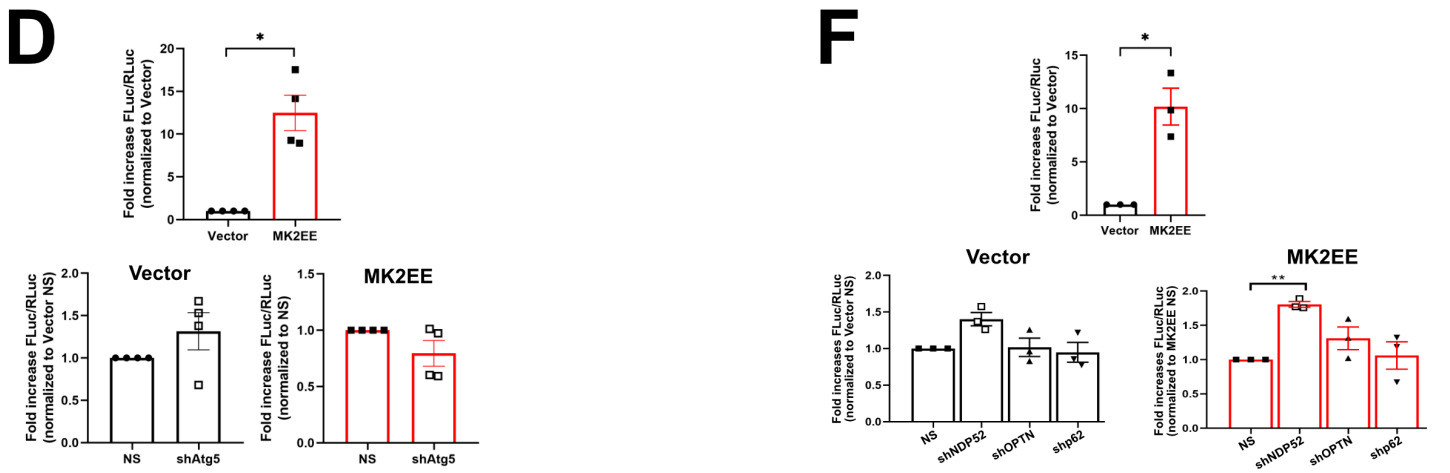
D
Fold increase FLuc/RLuc (normalized to Vector)
Vector
MK2EE
Vector
Fold increase FLuc/RLuc (normalized to Vector NS)
NS
shAtg5
MK2EE
Fold increase FLuc/RLuc (normalized to NS)
NS
shAtg5
F
Fold increaes FLuc/Rluc (normalized to Vector)
Vector
MK2EE
Vector
Fold increases FLuc/RLuc (normalized to Vector NS)
NS
shNDP52
shOPTN
shp62
MK2EE
Fold increases FLuc/RLuc (normalized to MK2EE NS)
NS
shNDP52
shOPTN
shp62

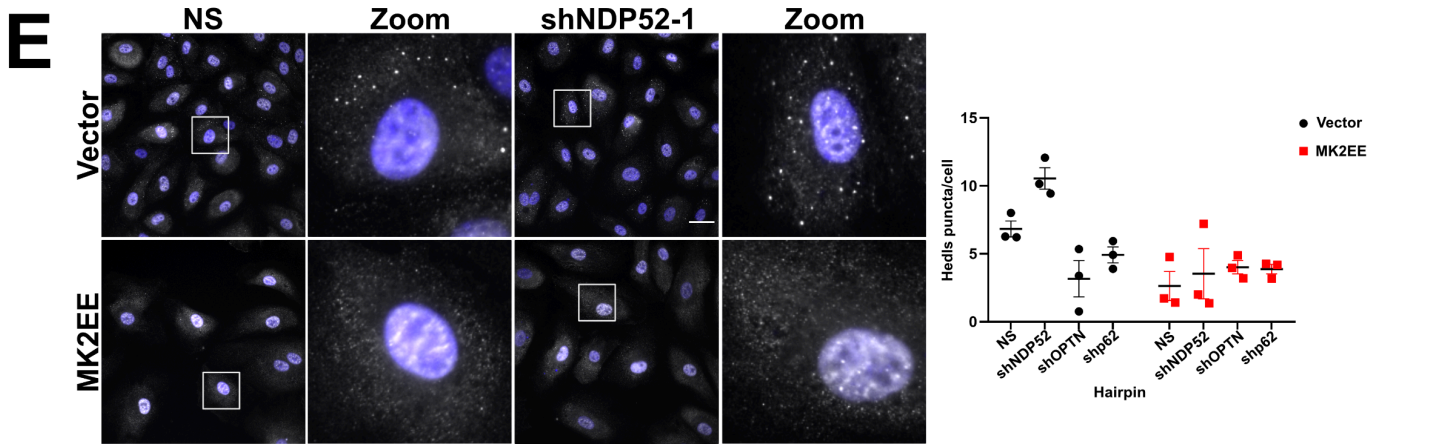
E
NS
Zoom
shNDP52-1
Zoom
Vector
MK2EE
Hedls puncta/cell
NS
shNDP52
shOPTN
shp62
NS
shNDP52
shOPTN
shp62
Hairpin
Vector
MK2EE

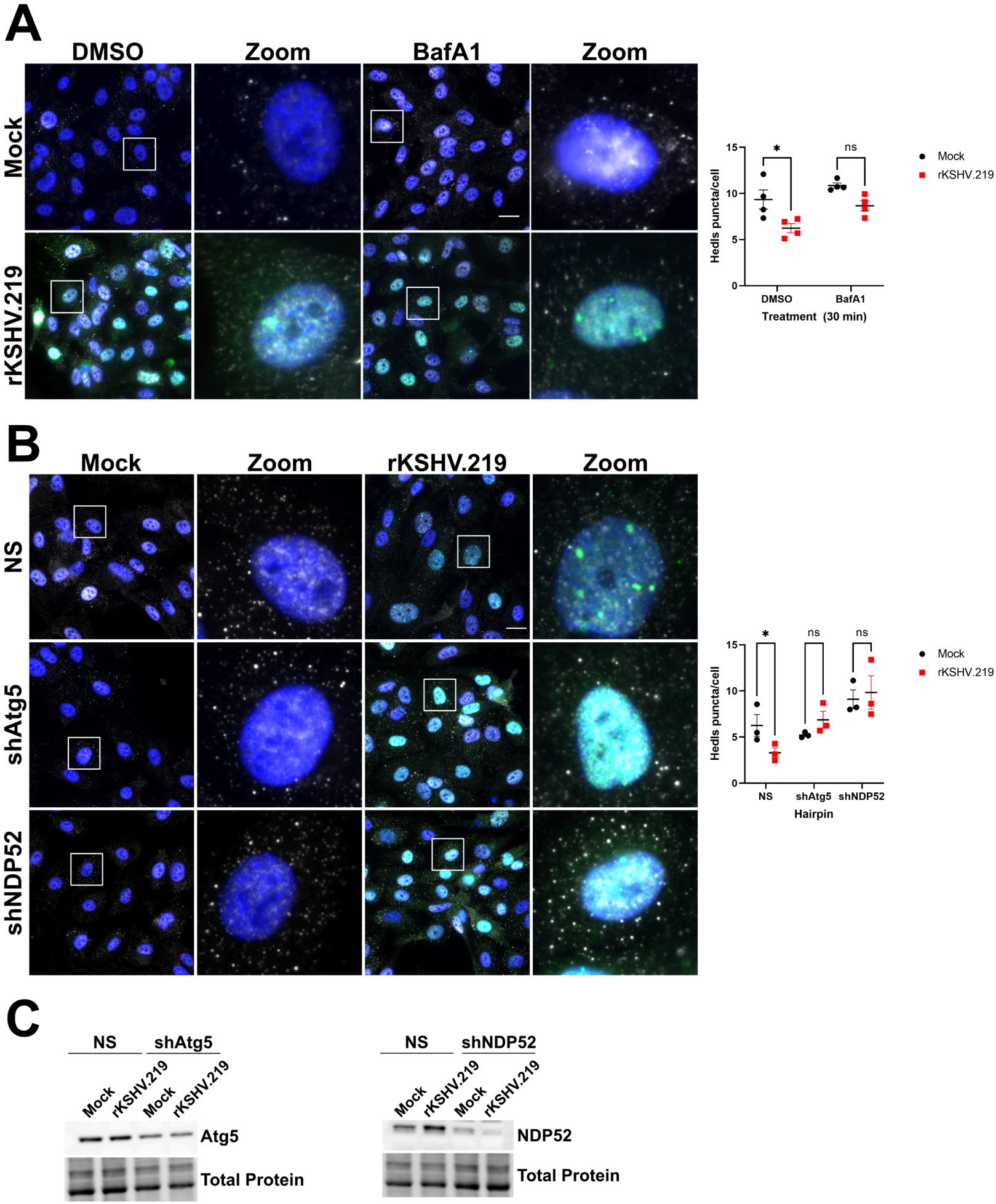
A
DMSO
Zoom
BafA1
Zoom
Mock
rKSHV.219
Hedls puncta/cell
15
10
5
0
*
ns
DMSO
BafA1
Treatment (30 min)
Mock
rKSHV.219
B
Mock
Zoom
rKSHV.219
Zoom
NS
shAtg5
shNDP52
Hedls puncta/cell
15
10
5
0
*
ns
ns
NS
shAtg5
shNDP52
Hairpin
Mock
rKSHV.219
C
NS
shAtg5
Mock
rKSHV.219
Mock
rKSHV.219
Atg5
Total Protein
NS
shNDP52
Mock
rKSHV.219
Mock
rKSHV.219
NDP52
Total Protein